Island Arc

*Island Arc* (2012) **21,** 118–147

Research Article

# Lateral variations in the lithology and organic chemistry of a black shale sequence on the Mesoarchean seafloor affected by hydrothermal processes: The Dixon Island Formation of the coastal Pilbara Terrane, Western Australia

SHOICHI KIYOKAWA,[1,2]* TAKASHI ITO,[3] MINORU IKEHARA,[4] KOSEI E. YAMAGUCHI,[5,6] SHOICHIRO KOGE[1] AND RYO SAKAMOTO[1]

[1]*Department of Earth and Planetary Sciences, Kyushu University, Fukuoka, 813-8581, Japan (email: kiyokawa@geo.kyushu-u.ac.jp)*, [2]*Department of Geology, University of Johannesburg, Auckland Park 2006, Johannesburg, South Africa*, [3]*Faculty of Education, Ibaraki University, Mito, 310-8512, Japan*, [4]*Center for Advanced Marine Core Research, Kochi University, Nankoku, 783-8502, Japan*, [5]*Department of Chemistry, Toho University, Funabashi, 274-8510, Japan, and* [6]*NASA Astrobiology Institute*

**Abstract** The Dixon Island Formation of the coastal Pilbara Terrane, Western Australia is a 3.2 Ga volcanic–sedimentary sequence influenced by syndepositional hydrothermal activity formed in an island-arc setting. We documented lateral variations in stratigraphy, hydrothermal alteration, and biological activity recorded in the sedimentary rocks (over several kilometers), with the aim of identifying areas of biological activity and related small-scale structures. The Dixon Island Formation comprises volcaniclastics, black chert, and iron-rich chert within seven tectonic blocks. Based on detailed geological mapping, stratigraphic columns, carbon isotope composition, and organic carbon ($C_{org}$) content, we found lateral (>5 km) variations in stratigraphy and carbon isotope compositions in a black chert sequence above the Mesoarchean seafloor with hydrothermal activity. Two felsic tuff layers are used as stratigraphic marker beds within a black chert sequence, which was deposited on altered volcanic rocks. The black chert sequence in each tectonic block is 10–20 m thick. Thickness variations reflect topographical undulations in the paleo-ocean floor due to faulting. Early-stage normal faults indicate extensional conditions after hydrothermal activity. Black chert beds in the topographically subsided area contain higher $C_{org}$ contents (about 0.4 wt%) than in areas around the depression (<0.1 wt%). Carbon isotope compositions for the black chert vary from –40 to –25‰, which are similar to values obtained for a black chert vein within the komatiite–rhyolite tuff sequence (underlying the black chert sequence). Those for other rock types in the Dixon Island Formation are –33 to –15‰. Results indicate that deformation occurred soon after the final stages of hydrothermal activity. After this early-stage deformation, organic-rich sediments were deposited over an area several kilometers across. The organic-rich sediments indicate stagnant anoxic conditions that resulted in the deposition of siliceous and organic matter from hydrothermal vein systems. When hydrothermal activity terminated, normal faulting occurred and organic matter was deposited from the sea surface and silica from the seafloor.

**Key words:** Archean, carbon isotopes, black chert, black chert vein, greenstone belt, hydrothermal system, komatiite, normal fault.

*Correspondence.

Received 11 June 2011; accepted for publication 14 March 2012.



doi:10.1111/j.1440-1738.2012.00811.x

## INTRODUCTION

Archean greenstone belts contain volcanic rocks, siliciclastics, and chemical sediments that consist mainly of hydrothermal sedimentary sequences deposited during a hiatus in volcanism (e.g. Lowe 1999; Van Kranendonk 2006). It is important to recognize such volcanic–chemical sedimentary sequences in Archean oceanic and surface environments, because they may contain organic-rich hydrothermal vein systems (e.g. Ueno *et al.* 2004; Van Kranendonk 2006; Van Kranendonk *et al.* 2007).

Vertical stratigraphic changes in chemical sedimentary sequences have been identified in the east Pilbara of Australia and in the Barberton Greenstone Belt in South Africa and Swaziland (e.g. Lowe & Byerly 1999; Van Kranendonk *et al.* 2007). Based on detailed geological mapping, correlative sequences have been documented in several places: the Buck Reef chert area in Barberton (de Ronde *et al.* 1994; Lowe & Byerly 1999; de Vries *et al.* 2006), the North Pole dome area (Kitajima *et al.* 2001; Terabayashi *et al.* 2003), the Marble Bar chert area (Van Kranendonk 2006), and the Panorama district (Brauhart *et al.* 1998, 2001) in the east Pilbara, Australia. The development of chemical sediment sequences in most of these areas was controlled by normal faults and growth faults along which hydrothermal vein systems formed (de Ronde *et al.* 1994; Nijman *et al.* 1999; Kitajima *et al.* 2001). However, these areas show limited outcrops because of vegetation cover, which obscures information on lateral variations in the nature of cover sediments on the Archean ocean floor. Detailed, continuous information on the paleo-ocean floor is important for the recognition of hydrothermal fluid pathways within volcanic rocks and to understand the conditions of the ocean floor surface above hydrothermal vent systems.

The Dixon Island Formation, on Dixon Island, Western Australia, is one of the best-preserved and most continuous outcrops of Mesoarchean volcanic–sedimentary sequences worldwide (Fig. 1). This area, situated within the coastal Pilbara Terrane or West Pilbara Superterrane (Krapez & Eisenlohr 1998; Kiyokawa *et al.* 2002; Smithies *et al.* 2005; Van Kranendonk *et al.* 2007), is interpreted as a 3.2–3.0 Ga collision- and accretion-related tectonic sequence bounded by the right-lateral strike-slip Sholl Shear Zone (Krapez & Barley 1987; Kiyokawa *et al.* 2002; Van Kranendonk *et al.* 2007; Hickman 2012).

The Dixon Island Formation is one of the least metamorphosed sequences in the Pilbara Terrane, and there is >5 km of continuous non-vegetated outcrop along the northern coast of the island (Fig. 1b). The stratigraphy of the Dixon Island Formation and the overlying iron-formation-rich Cleaverville Formation has been reported in detail by Kiyokawa and Taira (1998) and Kiyokawa *et al.* (2006), which include (from lower to upper top): Lagoon Pillow Basalt, Dixon Island Formation, Dixon Pillow Basalt, and Snapper Beach Formation (herein referred to as the Cleaverville Formation). The Dixon Island Formation overlies a very thick pillow basalt sequence (the Lagoon Pillow Basalts) preserved on the southern side of a large syncline (Kiyokawa & Taira 1998). The pillow basalt sequence consists of mid-ocean ridge basalt (MORB)-type basalts and was highly altered during the early stages of hydrothermal alteration (Ohta *et al.* 1998; Shibuya *et al.* 2007). Our detailed mapping and measurements of younging directions within the pillow basalts and within the sediments between the Cleaverville Formation and the Lagoon Pillow Basalt sequence have revealed a large synclinal structure (the Cleaverville syncline) and the stratigraphic position of the Dixon Island Formation within the thick pillow basalt sequence (Fig. 1). The axial section of the syncline is affected by left-lateral strike-slip faulting and is sandwiched between sandstone- and black chert-bearing shallow-water sedimentary sequences (Kiyokawa & Taira 1998; Kiyokawa *et al.* 2002).

The stratigraphy of the Dixon Island and Cleaverville Formations is well preserved on the northern limb of the Cleaverville syncline. The former, which is interpreted as a hydrothermal ocean-floor sequence within an immature island-arc system (Kiyokawa *et al.* 2002), is 300–400 m thick and consists of three members (from lower to upper): the Komatiite–Rhyolite Tuff Member, the Black Chert Member, and the Varicolored Chert Member. The Dixon Pillow Basalt sequence, which does not contain vesicles, consists of well-preserved pillow lavas that conformably overlie the Varicolored Chert Member (Fig. 2). This basalt has been named the 'Port Robinson basalt' by the Geological Survey of Western Australia (Hickman 2012). The upper part of the Komatiite–Rhyolite Tuff Member represents ocean-floor volcanism within the immature island-arc (Kiyokawa & Taira 1998; Kiyokawa *et al.* 2002).

The Dixon Island Formation is well preserved along both the Cleaverville coast and the Dixon Island coast (Fig. 1). In total, 10 blocks are recog-

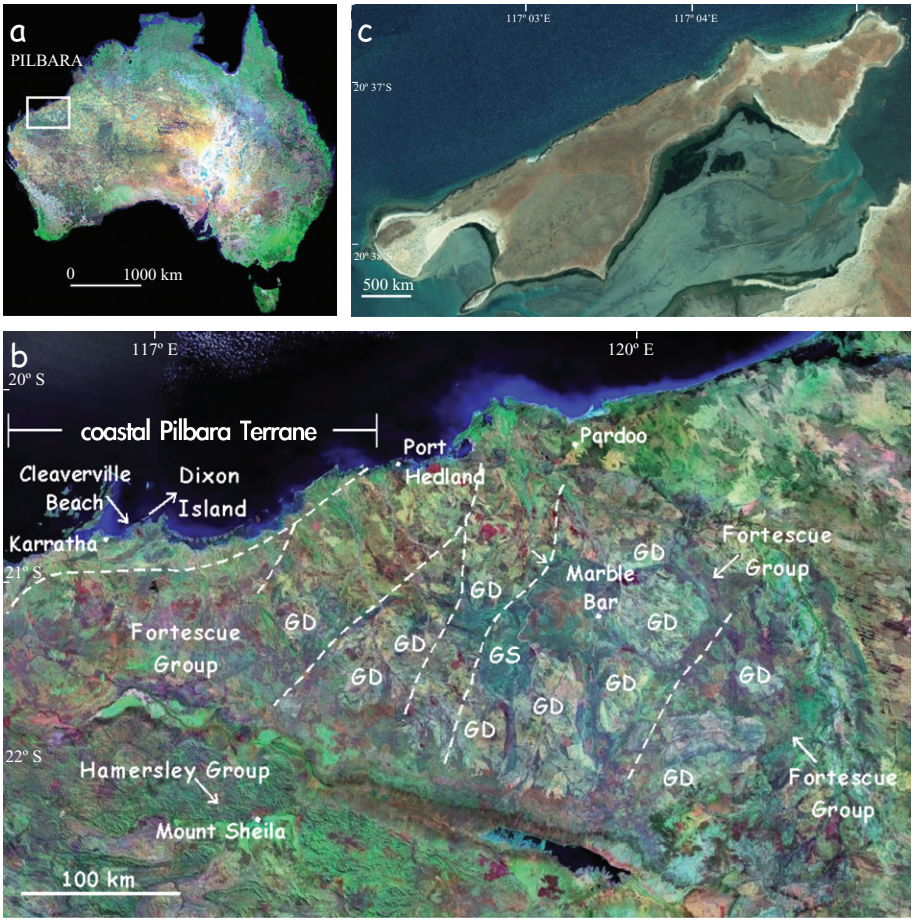


**Fig. 1** (a) Landsat ETM 742 mosaic of Australia. The mosaic is comprised of 369 individual Landsat satellite image acquired between July 1999 and September 2000 (Courtesy of ACRES, Geoscience Australia). Rectangle indicates area covered in (b). (b) Landsat ETM 742 image showing the general geological units of the Pilbara granitoid–greenstone terrane. The Fortescue and Hamersley Groups bound the granitiod–greenstone terrane on either side. (c) Landsat TM 321 image of Dixon Island. (d) Geological map of the Cleaverville area (from Kiyokawa *et al.* 2006). CL A to CL D are tectonic blocks bounded by strike-slip faults. (e) Geological map of the Dixon Island. DX A to DX F are tectonic blocks bounded by strike-slip faults GD, granitoid dome; GS, greenstone belt.

nized within the formation along the northern coast of Dixon Island (blocks DX A–F; Fig. 1) and along Cleaverville Beach (blocks CL A–D; Fig. 1). The northern coast of Dixon Island contains especially well-preserved outcrops, where the rocks are less deformed than those at Cleaverville Beach (Fig. 1b). Lithological contacts and the nature of lateral changes in stratigraphy, however, are obscure within the Komatiite–Rhyolite Tuff and Black Chert members. The degree of alteration of volcanic rocks and the thickness of the overlying black chert sequence vary along the boundary between the Komatiite–Rhyolite Tuff and Black Chert members, because of the variable distribution of hydrothermal black chert veins.

In this study, we outline the nature of lateral stratigraphic variations within low-temperature hydrothermal environments in a relatively deep oceanic environment at 3.2 Ga. Stratigraphic sections reconstructed for a 5 km-wide area show in detail the nature of lateral variations in seafloor stratigraphy. In particular, we focus on lateral changes in the sedimentary sequence above volcanic rocks, the continuity of key felsic tuff beds and the nature of their contacts, and geochemical and isotopic analyses of organic-rich rocks, as well as their organic carbon contents. We thus aim to reconstruct in detail the ancient ocean-floor environment influenced by syndepositional hydrothermal activity represented by the Dixon Island Formation.

## TECTONIC SETTING AND DEFORMATION EVENTS

The coastal Pilbara Terrane (Fig. 1c; Kiyokawa *et al.* 2002) is one of the best-preserved Archean greenstone belts in the Pilbara granitoid–

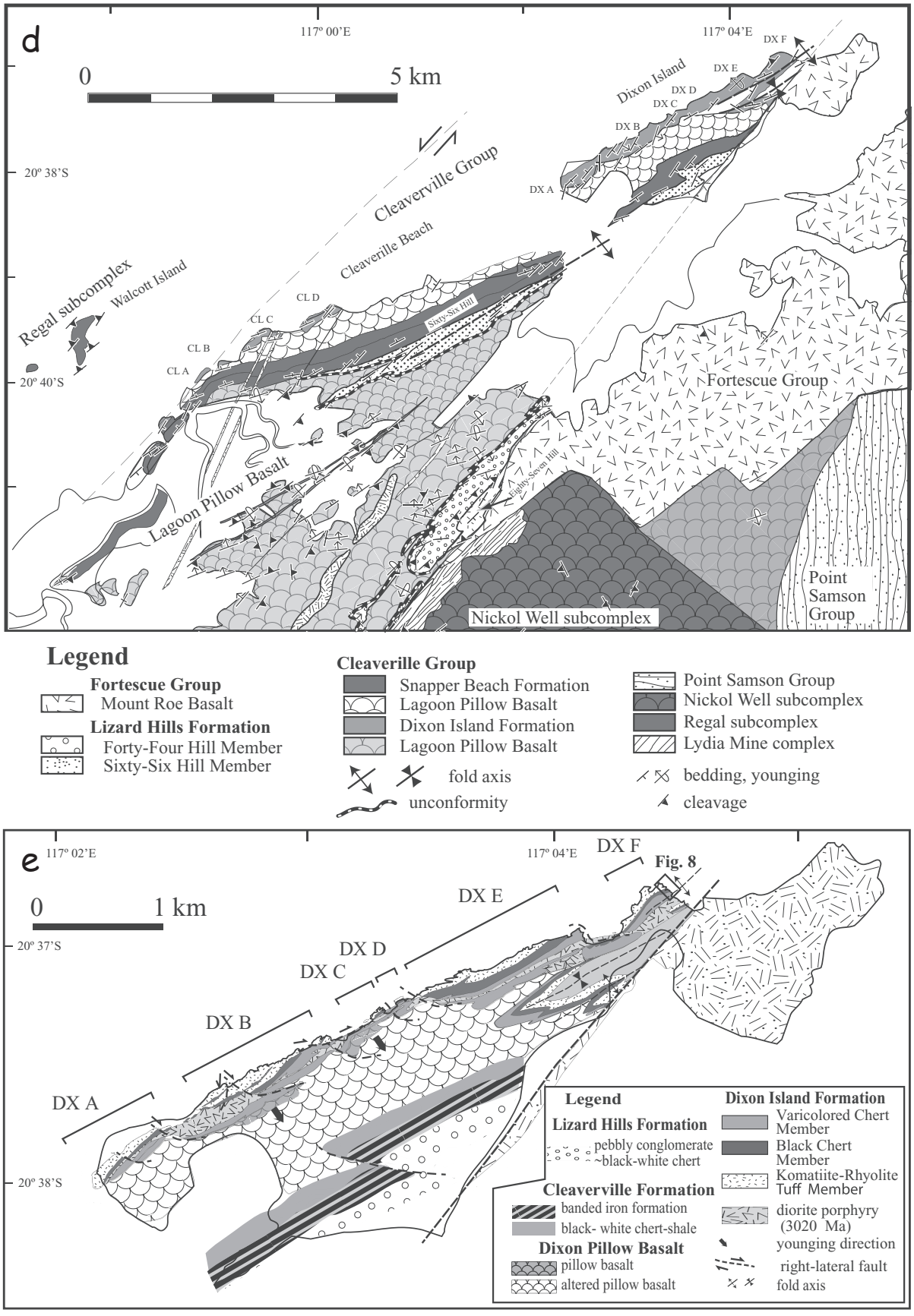


**Fig. 1** *Continued*

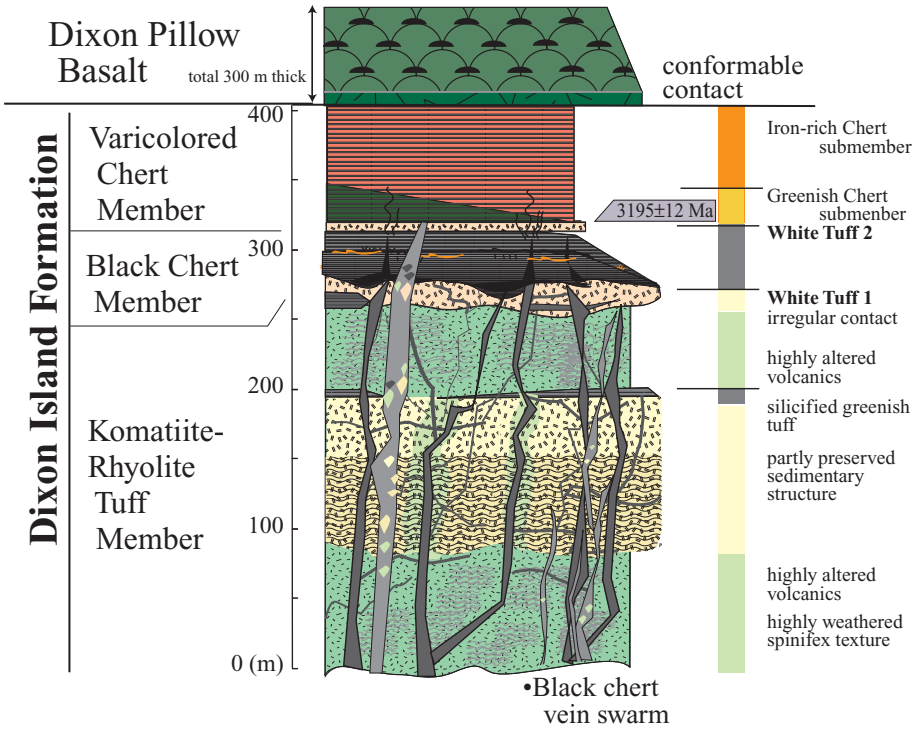


**Fig. 2** Stratigraphic column of the Dixon Island Formation (modified after Kiyokawa *et al.* 2006).

greenstone terrane. Several tectonic models have been proposed to explain the origin of this terrane, including a rifted basin (Horwitz 1990), accreted oceanic crust (Ohta *et al.* 1998), and collision between an immature arc and a continent (Kiyokawa *et al.* 2002). The rifted basin model is not well supported because the lowermost units in the sequence are thick pillow basalts. Ohta *et al.* (1998) identified MORB-type volcanic rocks in the terrane based on mineralogy (clinopyroxene), and interpreted them as accreted ocean crust. However, based on detailed geological mapping and data on younging directions, the Cleaverville Beach area contains a syncline that preserves the original stratigraphy, unaffected by the thrust fault of the accretionary prism model proposed by Ohta *et al.* (1998). Kiyokawa *et al.* (2002) reported a cyclic volcanic–sedimentary sequence in the Pilbara granitoid–greenstone terrane that was deposited at 3.19 Ga, interpreted to represent an accreted thrust sheet emplaced on the 3.27 Ga Karratha granitoid (Smith *et al.* 1998; Kiyokawa *et al.* 2002). The Dixon Island and Cleaverville Formations, which are the lowest-metamorphic-grade volcanic–sedimentary sequences in the Pilbara granitoid–greenstone terrane, are among the best-preserved sequences in the thrust sheets of the terrane.

Detailed structural work has revealed three deformation events in the coastal Pilbara Terrane (Kiyokawa *et al.* 2002). $D_1$ resulted from collision between an immature island arc and micro-continental crust at 3.2–3.1 Ga. $D_2$ records regional-scale left-lateral strike-slip faulting at 3.02–2.92 Ga, and $D_3$ involved localized right-lateral strike-slip faulting (along the Sholl Fault) at 2.92–2.77 Ga. $D_2$ left-lateral deformation strongly affected the present coastal regions of the Pilbara Terrane. In the Cleaverville–Dixon Island region, a diamond-shaped area of low-metamorphic-grade pillow basalt is bounded by a shallow-water sedimentary sequence (Lizard Hills Formation; Kiyokawa & Taira 1998; Kiyokawa *et al.* 2002). Outcrop-scale left-lateral asymmetric deformation structures (folds and faults) occur along the Cleaverville–Dixon Island coast. This diamond-shaped distribution of low-grade metamorphism (prehnite–pumpellyite facies), which is surrounded by amphibolite facies lithological units, may be interpreted as a pull-apart basin structure (Kiyokawa *et al.* 2002). The distribution of rocks of various metamorphic grades indicates that the area in the basin subsided by less than 5 km relative to surrounding rocks during a period of left-lateral faulting.

The deformation events recorded by the Dixon Island Formation are as follows: (i) $D_1$ resulted in map- and outcrop-scale asymmetric folds with horizontal fold axes ($F_1$); and (ii) $D_2$ produced asymmetric folds ($F_2$) with vertical fold axes,

with block boundaries defined by right-lateral strike-slip faults (Kiyokawa *et al.* 2002). Each block on Dixon Island (DX A–F) has been rotated counter-clockwise by 20–30° due to regional left-lateral $D_2$ events.

Detailed mapping along the Dixon Island coast has revealed pre-$D_1$ normal faults ($F_0$) in the DX B block (Fig. 3) that strike northwest–southeast. The faults are marked by zones of fault gouge (0.5–1.0 cm thick), have cohesive contacts, and branch within altered volcanic rocks and bedded cherty sediments of the Komatiite–Rhyolite Tuff Member (Fig. 4a,b). The $F_0$ faults are deformed by map-scale $F_1$ folds and are truncated by $D_2$ right-lateral strike-slip faults. Black chert beds within the altered komatiite volcanic rocks are displaced by more than 5 m along $F_0$ faults. By restoring $D_1$-deformed, steeply inclined beds back to horizontal, it is apparent that the $F_0$ faults were normal faults. There are no hydrothermal vein systems along $F_0$ faults. To understand the relationship between the activity of $F_0$ faults and hydrothermal vein systems, it is important to constrain the stratigraphy and thickness of the sediments that overlie the volcanics.

## STRATIGRAPHY

The stratigraphy of the Dixon Island Formation is best preserved in the DX B and DX C blocks. In this section, we describe in detail the stratigraphic units in these blocks and their lateral variations, and then compare the units with the stratigraphic sequence observed in other blocks (DX A, DX D, DX E, and DX F).

The Komatiite–Rhyolite Tuff Member (the Rhyolite Tuff Member of Kiyokawa *et al.* 2006), which is best preserved in the DX B and DX E blocks (Fig. 3), contains highly altered komatiite, pale green silicified basic tuff, well-laminated black chert, and whitish felsic tuff. The member preserves two cycles of highly altered komatiite lavas and well-stratified rhyolite tuff, and consists of three units: (i) green to brown, highly altered volcanic rocks; (ii) silicified, finely laminated, greenish and white tuff; and (iii) laminated black chert beds. Scanning electron microscope–energy dispersive X-ray spectrometry (SEM-EDS) analyses of the green to brown, highly altered volcanic rocks indicate that they contain dendritic crystals of Cr-spinel, which is usually found in basic rocks (Fig. 4). This result supports the interpretation that the green-brown volcanic rocks are highly altered komatiite lavas and ultramafic volcanic tuffs. The 'splashed pattern fabrics' within the green volcanic rocks described by Kiyokawa *et al.* (2006), which consist of aggregates of highly silicified sheet-like crystals, are re-interpreted here as spinifex texture (Fig. 4). The pale greenish siliceous komatiite volcanic rocks resemble the komatiite volcaniclastic rocks of the Hooggenoeg and Kromberg Formations of the Barberton Greenstone Belt (e.g. Lowe 1999; Lowe & Worrell 1999). Based on detailed geological mapping, we identified lateral variations in composition and texture in this altered zone that may relate to hydrothermal circulation beneath the vent system.

The white felsic tuff beds of the upper part of the Komatiite–Rhyolite Tuff Member contain fine-grained pseudomorphs of volcanic glass. This white felsic tuff, which is referred to here as White Tuff 1, is well bedded and locally massive. The lateral extent and nature of White Tuff 1 provide clues to the condition of the paleo-seafloor.

Organic-matter-bearing black silica dikes, which are here referred to as 'black chert veins' (following Kiyokawa *et al.* 2006), are well preserved in large sections of the Komatiite–Rhyolite Tuff Member. The veins occur as two types: Type 1 veins are massive and organic-rich, whereas Type 2 veins are silica-rich and organic-poor, and contain fragments of black chert and siliceous volcanic breccia wall rock (Kiyokawa *et al.* 2006). Both vein types are equally abundant in each block on Dixon Island (Kiyokawa & Taira 1998).

The Black Chert Member is a black chert bed (10–20 m thick) on top of White Tuff 1. Five rock types have been identified in the Black Chert Member: massive black chert, laminated black chert, greenish siliceous shale, iron-rich red shale, and white felsic tuff. The upper part of this member consists of 1–2 m of white felsic tuff (referred to here as White Tuff 2) that is well laminated and contains gray to red mudstone beds.

The Varicolored Chert Member is 100–300 m thick and consists of well-stratified laminated white, red, and black chert, and banded iron formation. Each lamina is less than 1 mm thick and there are no detrital grains. No black chert veins were observed in this member. The Dixon Pillow Basalt conformably overlies these hydrothermal deposits.

## CHARACTERISTICS OF TECTONIC BLOCKS OF THE DIXON ISLAND FORMATION

To understand the nature of lateral variations in the three members of the Dixon Island Formation,

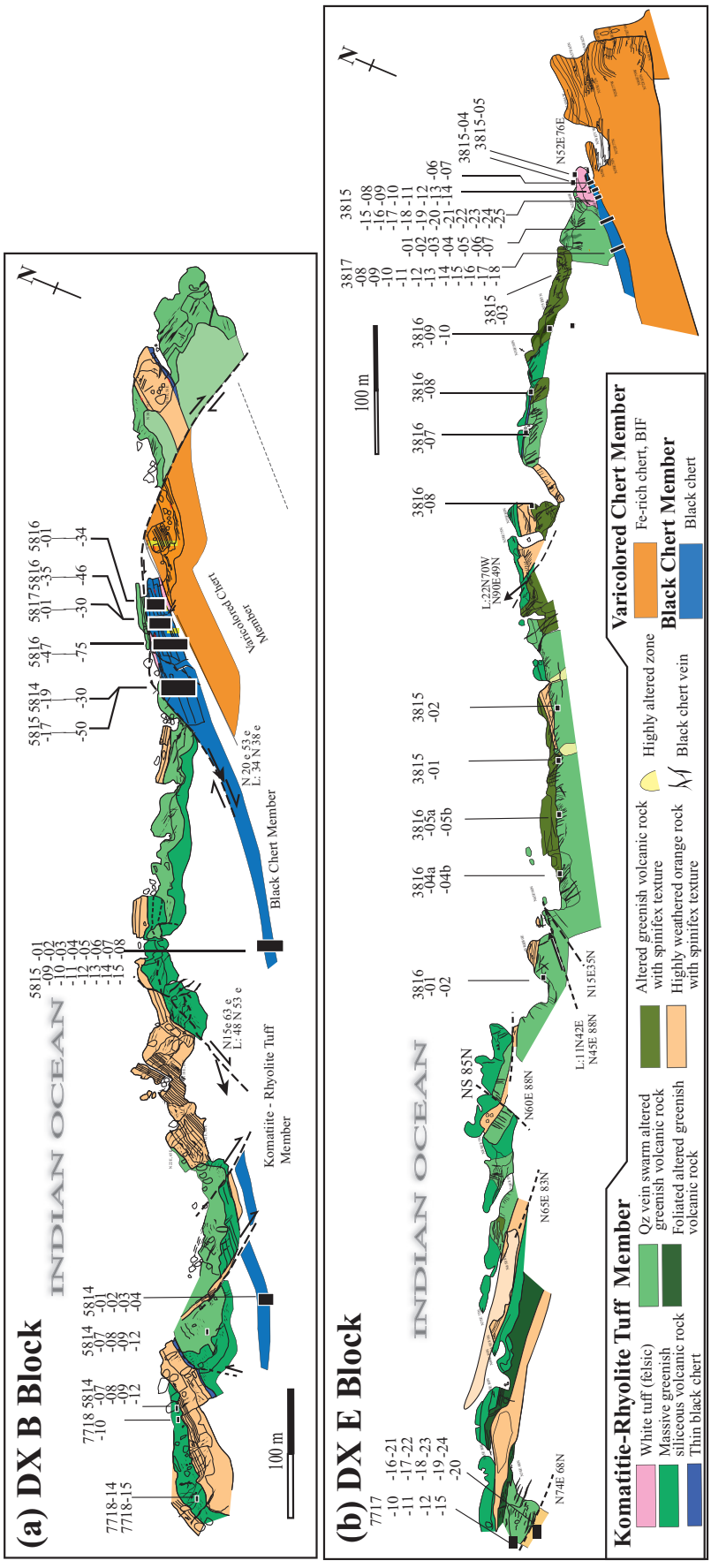


**Fig. 3** Route maps of the DX B (a) and DX E (b) blocks in the Dixon Island Formation, respectively. Numbers indicate sampling points.

**Fig. 4** (a) Overview photograph of a highly altered komatiite tuff bed and thin black chert bed within the Komatiite–Rhyolite Tuff Member. White dashed lines show early-stage normal faults that truncate the black chert bed. (b) Detailed view of a normal fault within komatiite tuff beds and black chert beds. The fault is partly branched and a white fault gouge is preserved with slickensides. (c) Spinifex texture in altered komatiite lava. (d) Backscattered electron micrograph of Cr-spinel within the altered greenish komatiitic tuff.

we correlated the stratigraphy between each of the six tectonic blocks on Dixon Island. We describe the characteristics of each block and deformation features, and summarize their stratigraphy (Fig. 5; Table 1), focusing on the thickness of the Black Chert Member, the occurrence of key marker beds (e.g. thick beds of volcanic tuff), the distribution of black chert veins, and the nature of hydrothermal alteration of the Komatiite–Rhyolite Tuff Member.

### DX A BLOCK

The DX A block, located in the western part of Dixon Island, is characterized by 500 m-long cherty hills that form continuous exposures along the west and northwest coast. Because of poor exposure and the effects of $D_2$ deformation, the stratigraphy of the DX A block remains poorly constrained. Early-stage ($D_1$) folding is recognized in inland areas, within the Varicolored Chert Member. The Komatiite–Rhyolite Tuff Member is exposed along a >100 m-wide section along the coast. The Black Chert Member is less than 7 m thick. White Tuff 1 consists of tuff breccia (several meters thick) that conformably overlies highly altered greenish volcanic siliceous rocks of the Komatiite–Rhyolite Tuff Member.

### DX B BLOCK

The DX B block is characterized by several hills (30–50 m in relief) along a 1200 m coastal section, and is bounded to the west and east by the $D_2$ strike-slip faults (Kiyokawa *et al.* 2006). The stratigraphy and distribution of members in the DX B block, as summarized below, is presented in detail by Kiyokawa *et al.* (2006). The DX B block is subdivided into three (east, middle, and west) domains by $D_2$ strike-slip faults. The middle and west domains are composed mainly of the Komatiite–Rhyolite Tuff Member, whereas the east domain contains the Komatiite–Rhyolite Tuff, Black Chert, and Varicolored members, with the Black Chert Member being dominant. In the west domain, the Komatiite–Rhyolite Tuff Member contains early-stage normal faults.

The Komatiite–Rhyolite Tuff Member in the DX B block contains alternating, altered greenish-brown komatiitic volcanic rocks, silicified tuff beds, and thin black chert beds, locally affected by intense hydrothermal alteration. Well-preserved swarms of black chert veins are well exposed within greenish, silicified volcanic rocks that locally show spinifex texture.

White Tuff 1, which is 1–2 m thick, occurs above well-stratified, greenish, fine tuff beds in the east domain (Fig. 6a). Three units are identified within the Black Chert Member (from lower to upper): (i) thick, massive black chert with fine-grained pyrite crystals; (ii) well-laminated black chert beds, layers of barite–aragonite pseudomorphs after quartz, thin iron-rich red chert beds, and yellow-brown biomat layers (Fig. 7a); and (iii) bedded black and white chert with thin layers of iron formation. White Tuff 2, which consists of well-laminated white tuff and thin red iron-rich shale, forms the top of this member. White Tuff 2 exceeds 2–3 m in thickness and is locally offset along strike-slip faults.

The Varicolored Chert Member, which overlies White Tuff 2, consists of well-laminated black and white chert beds, and beds of chert-rich iron formation. The laminations (<0.1 mm thick) consist of organic-rich black chert, silica-rich chert, and iron-rich zones.

### DX C BLOCK

The DX C block is bordered by the Dixon Pillow Basalt to the west and by a small cove to the east, which may have developed at the site of an early-stage normal fault. The well-preserved, continuous stratigraphy of the lower to middle parts of the Dixon Island Formation has been identified on the east side of the DX C block (Kiyokawa *et al.* 2006).

The Komatiite–Rhyolite Tuff Member, which is well exposed along the coastal part of the DX C block, is similar in lithology to equivalent rocks in the DX B block. Many black chert veins are well preserved in the member. White Tuff 1 (2–3 m thick) contains numerous veins of black chert in its lowermost portion, obscuring the lower boundary, and a partly preserved intensive glassy texture is observed in interbedded white tuff and black-gray chert (Fig. 7b).

The DX C block also contains the well-stratified Black Chert Member (Kiyokawa *et al.* 2006). White Tuff 2 conformably overlies bedded black chert and is overlain in turn by hematite-bearing well-laminated black–white chert. In this block, the tuff is an undeformed, well-bedded white-gray felsic tuff 3 m thick. The Varicolored Chert Member is well exposed in the lower half in this block, along the coast. The gray chert beds of this member contain a 1 m-thick interval of well-laminated black chert beds.

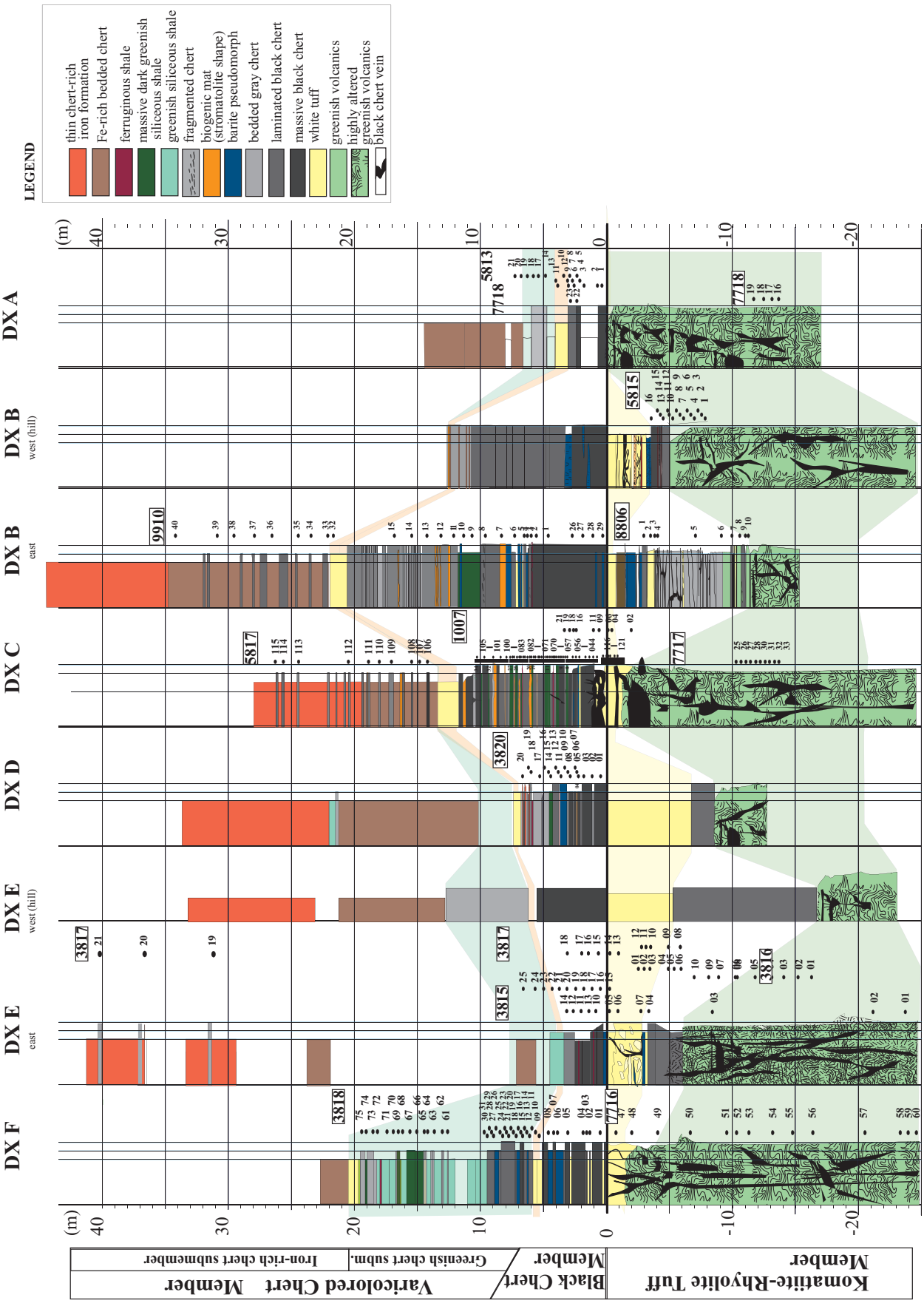


**Fig. 5** Stratigraphic columns of component blocks in the Dixon Island Formation. Numbers show sampling levels. Columns for the DX B and DX C blocks are based on Kiyokawa *et al.* (2006).

**Table 1** Summary of stratigraphic characteristics of each block on Dixon Island

| Characteristics of the block | Category | DX A | DX B | DX C | DX D | DX E | DX F |
|---|---|---|---|---|---|---|---|
| General character | Distribution length | 500 m | 1200 m (30–50 m hill with cliff) (500 m east from DX A) | About 250 m wide (500 m east from DX B) | 50 m (50 m east from DX C) | 1200 m | 150 m |
| | Exposed area | West and northwest coast | Northern coast and hill | Along the coast and hill | Along the coast | Along the coast | Along the east coast |
| | Exposed level | Not so good (north side has beach) | Excellent well-preserved, continuous stratigraphy whole section | Excellent: well-preserved, continuous stratigraphy | Excellent: well-preserved, continuous stratigraphy at lower section | Excellent: well-preserved, continuous stratigraphy | Excellent: well-preserved, continuous stratigraphy |
| | Stratigraphy | Poorly constructed | Excellent preserved whole section | Excellent preserved lower-middle section | Excellent preserved whole section | Excellent preserved whole section | Excellent preserved whole section |
| | Domain | One domain | Three domains: east, middle, west: right-lateral fault and lithology | One domain | Two domains: NE–SW-striking right-lateral fault: offset by more than 9 m | Three domains: east, middle, west (lithology and topography) | One domain |
| Komatiite–Rhyolite Tuff Member | Distribution | Northwest coast | East, middle, west domains >800 m of coastline with steep cliffs | North coast | North coast | West coast | North and east coast |
| | Thickness | >50 m | 200 m | >50 m | >10 m | Several hundred meters | 100 m |
| | Lithology | Massive, pale green siliceous rock | Altered greenish-brown komatiitic volcanic rock, silicified tuff beds and thin black chert bed | Highly altered and silicified greenish komatiitic volcanic rocks with pseudomorphs of spinifex texture and siliceous pale green tuff beds | Silicified greenish komatiitic volcanic rocks | Altered greenish-brown komatiitic volcanic rock, silicified tuff beds and thin black chert bed. Spinifex sequence several hundred meters and >3–4 m in thickness, are generally overlain by highly altered, greenish komatiitic rocks | Highly altered, pale green volcanic rocks |
| | White quartz vein | Few | Common | Common | Less | Common | Common |
| | Black chert vein | Thick black chert veins (>100 m-wide area) | Thick black chert veins and vein swam (>800 m area) | Thick black chert veins and vein swam (>100 m area) | Black chert veins (>50 m area) | Thick black chert veins and vein swam (>800 m) | Thick black chert veins and vein swam (>100 m) |
| | Hydrothermal alteration | Altered green silicified volcanics | Partly highly intense hydrothermal alteration with quartz and black chert veins | Partly highly intense hydrothermal alteration with quartz and black chert veins | Highly silicified rock | Partly highly intense hydrothermal alteration with quartz and black chert veins | Contains many black chert veins and is itself strongly altered (Fig. 7e) |
| | White Tuff 1 | White tuff with tuff breccia | Well bedded white tuff | Well bedded white tuff: partly preserved intensive glassy texture in its interbedded white tuff and black-gray chert stratigraphy (Fig. 7b) | Massive, coarse-grained white tuff void of black chert veins | Massive, coarse-grained white tuff void of black chert veins | Massive, coarse-grained white tuff with many veins |
| | Thickness | 1–3 m thick | 1–2 m thick | 2–3 m thick | 9 m thick (thickest) | 4–7 m thick | 1–3 m thick |

| | | | | | | | |
|---|---|---|---|---|---|---|---|
| | Continuous distribution | 3–4 m (inland outcrops) | 50 m (excellent continuous outcrop along the coast) 3–5 m (sporadically exposed at the hill top of west) | 20 m along the coast | 50 m along the coast | 70 m along the coast to hill top | 30 m along the coast |
| | Base rock | Highly altered greenish volcanic siliceous rock | Conformably contact with well-stratified greenish, fine tuff bed (east domain). Massive, homogeneous, fine-grained, and has a glassy texture | The lowermost portion of this bed contains numerous veins of black chert, which obscure the lower boundary of White Tuff 1 | Massive, coarse-grained white tuff void of black chert veins | Generally massive and is cut by black chert veins. East side preserved massive thick tuff bed | Altered volcanic zone, contains many black chert veins and is strongly altered (Fig. 7e). |
| Black Chert Member | Distribution | Northwest coast | East domain 120 m lateral change | North coast | North coast | East coast | North and east coast |
| | Thickness | Less than 7 m (west coast) | 20 m | 12 m | 10 m | <10 m | 10 m |
| | Lithology | Well-laminated black chert and comprises well-laminated black chert and tuff beds containing fragments of black chert (Fig. 5) | Lower: thick, massive black chert with fine-grained pyrite crystals | Lower: 5 m-thick, black and white chert beds, highly silicified barite–aragonite-barite pseudomorphs and felsic tuff layers | Lower: massive and laminated black chert and biomat beds | Lower: bedded and finely laminated black–white chert | Lower: bedded and massive black chert beds with thin white tuff beds |
| | | | Middle: well-laminated black chert beds, highly silicified barite-aragonite pseudomorphs layers which replaces quartz, thin iron-rich red chert beds, and yellow-brown biomat layers (Fig. 7a) | Middle: 4 m-thick, comprised of well-laminated black chert, dark green chert, and thin beds of red chert. Three yellowish-brown biomat beds within laminated black chert | Middle: well-laminated black chert and 20 cm-thick bedded massive black chert. Especially highly silicified yellowish-brown biomat bed. Altered, well-laminated black chert and thin beds of massive black chert | 10–20 cm-thick white chert beds. Many aragonite-barite pseudomorphs after fiber quartz within black and white chert | |
| | | | Upper: bedded black and white chert with thin layers of iron formation. Well-laminated white tuff and thin red iron-rich shale | Upper: 3 m-thick, well-laminated black chert, massive dark greenish chert, and minor Fe-rich ferruginous beds | Upper: well-laminated black chert with ferruginous layers | Upper: well-laminated black chert. Poorly exposed | Upper: laminated black chert beds and siliceous gray shale, along with several siliceous chert beds |
| | Aragonite pseudomorph | No | Common | Common | No | Aragonite with fan texture (Kiyokawa *et al.* 2006) | No |
| | Barite pseudomorphs | Few | Many beds (lower) | Many beds (lower) | Many beds (lower) | Many beds (lower) | Many beds (lower) |
| | Biomat bed | No | 30–50 m thick (one layer more than 100 m wide) | 20–50 cm thick (three layers) | 20–50 cm: highly silicified yellowish brown | No | No |
| | Stratigraphic relationship | Along the west coast, layer parallel fault preserved basal boundary. Upper boundary is not exposed | Conformable contact at upper and lower boundary | Conformable contact at upper and lower boundary | Conformably contact (east), strike-slip fault contact at west. West portion of this domain did not preserve whole black chert by strike-slip fault deformation. | Conformably contact of lower boundary at top of the hill. West portion of this domain did not preserve whole black chert by strike-slip fault deformation. East hill: poorly preserved along the coastal outcrops of the DX E block due to bedding-parallel strike-slip deformation | Along the west coast, layer parallel fault preserved basal boundary. Upper boundary is not exposed Weathered and forms a topographic depression (Fig. 7g) |

**Table 1** *Continued*

| Characteristics of the block | Category | DX A | DX B | DX C | DX D | DX E | DX F |
|---|---|---|---|---|---|---|---|
| | White Tuff 2 | Could not distinguish by folding | Well-laminated white tuff and thin red iron-rich shale | Well-laminated white tuff and thin red iron-rich shale | Well-stratified and laminated white felsic tuff | Well-stratified and laminated white felsic tuff | Highly altered white tuff with many black chert vein |
| | Thickness | >2 m<br>Locally deformed by strike-slip deformation | 2–3 m<br>Locally deformed by strike-slip deformation | 3 m<br>Conformably contacts, well-bedded white-gray felsic tuff | >3 m<br>Conformably contacts, well bedded white-gray felsic tuff | >2 m (strike-slip effect)<br>Conformably contacts, well bedded white-gray felsic tuff | >50 cm<br>Conformably contacts, well bedded white-gray felsic tuff |
| Varicolored Member | Distribution | Inland hill | East domain and hill top | West coast | West coast | West coast and hill | East coast |
| | Total thickness | More than 30 m (inland area) | >100 m | >15 m | >15 m | >100 m | >30 m |
| | Lithology | Thin laminated black-white chert and iron formation | Organic-rich black chert, silica-rich chert, and hematite-rich iron formation | Well-laminated gray and black chert, bedded chert, and thin hematite-rich iron formation<br>Gray chert beds contain a 1 m thick interval of well-laminated black chert beds | Well-laminated black-white-ferruginous bed and hematite-rich iron formation (partly folded) | Well-fine laminated black-white-ferruginous bed and iron formation<br>Lower: bedded and finely laminated greenish and white chert<br>Upper: very finely laminated chert and thin hematite iron beds | Well-bedded greenish shale/chert sequence and chert/BIF sequence<br>Lower: well-preserved, greenish bedded siliceous shale, dark greenish shale, and grey siliceous shale<br>Upper: Iron-rich chert and bedded chert |
| | Iron bed | Laminations (<1 mm thick) | Laminations (<1 mm thick) | Laminations (<1 mm thick) | Laminations (<1 mm thick) | Laminations (<0.1 mm thick) | Laminations (<1 mm thick) |
| | Greenish shale | Not well preserved | Massive dark greenish shale | Not well preserved | Not well preserved | Not well preserved | Well preserved |
| Dixon Pillow Basalt | | No | DX B hill south area, and DX B-DX C block coast | No (highly altered intrusion) | No (highly altered intrusion) | No (highly altered intrusion) | No (highly altered intrusion) |
| | Porphyry intrusion (bedding parallel) | Bedding-parallel porphyry intrusions at upper unit | Bedding-parallel porphyry intrusions at upper unit | Bedding-parallel porphyry intrusions at upper unit | Bedding-parallel porphyry intrusions at upper unit | Bedding-parallel porphyry intrusions at upper unit | Bedding-parallel porphyry intrusions at upper unit |
| Deformation | | $D_1$ horizontal axis fold, $D_2$ layer subparallel fault | $D_0$ normal fault, $D_2$ right lateral strike-slip faults | Small scale $D_0$ normal fault, $D_2$ right lateral strike-slip faults | $D_0$ vertical normal fault, $D_2$ bedding-subparallel northwest-dipping strike-slip fault. | $D_2$ bedding-subparallel northwest-dipping strike-slip fault. | Map-scale $D_1$ horizontal axis folds |

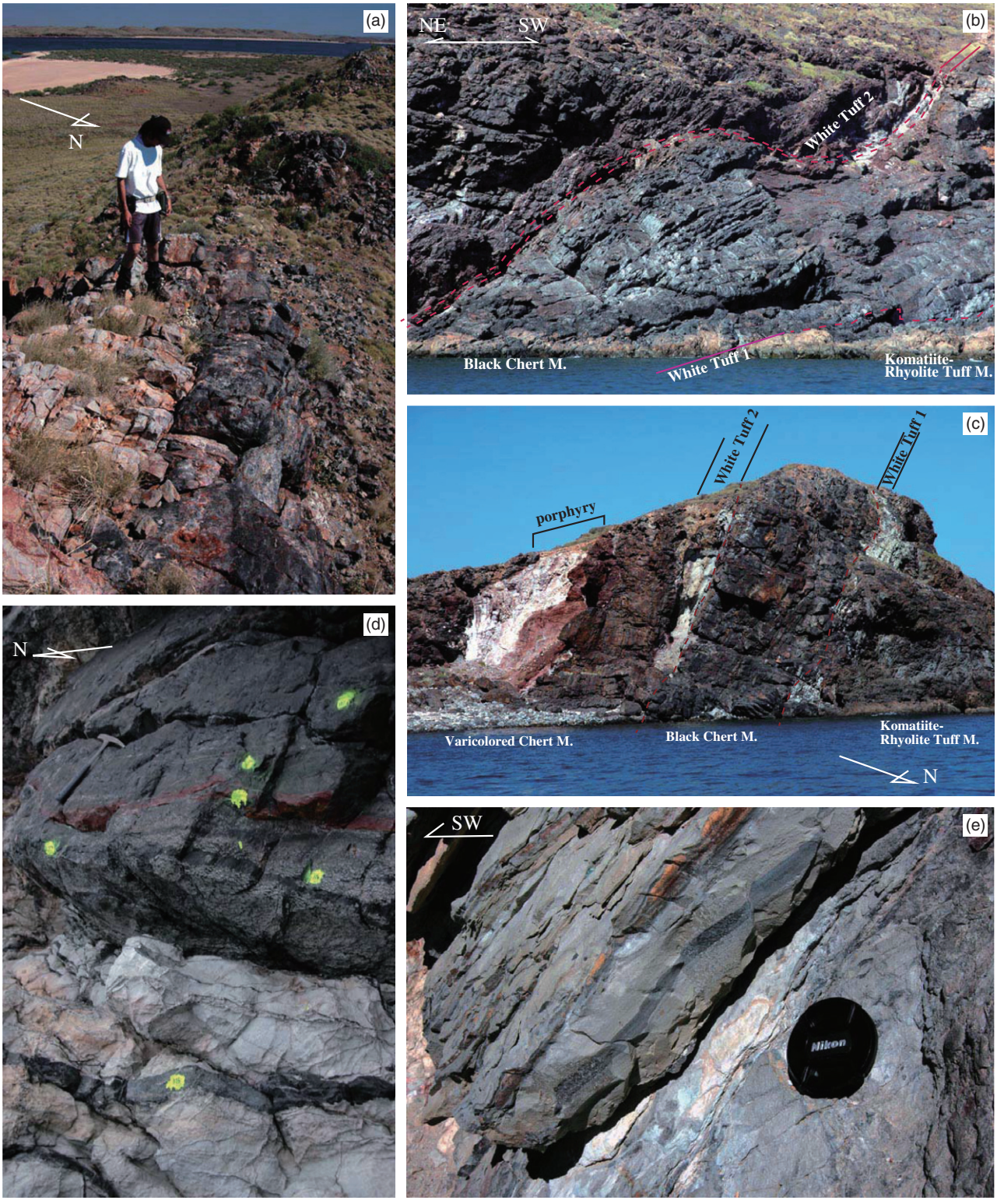


**Fig. 6** (a) View along bedding in White Tuff 1 in the uppermost part of the Komatiite–Rhyolite Tuff Member on the west side of the DX B block. White Tuff 1 occurs above the bedded black chert bed of the Komatiite–Rhyolite Tuff Member. Highly weathered volcanic rocks occur below the bedded black chert. (b) Overview of the east side of the DX B block. The hilltop is at about 30 m altitude. A 20 m-thick sequence of the Black Chert Member is well exposed in this section. The white-brown rock at left is highly weathered porphyry that was intruded subparallel to bedding. (c) Overview of the DX C block. White Tuff 1 and White Tuff 2 occur either side of a black chert sequence. The total thickness of the Black Chert Member is 13 m. (d) Contact between White Tuff 1 (about 2–3 m thick) and bedded massive black chert of the Black Chert Member in the DX C block. White Tuff 1 is cut by black chert veins, but bedding is still visible. This tuff is conformably overlain by massive black chert. The basal part of the black chert contains many glassy fragments and a red chert (jasper) bed. Yellow dots indicate sampling points. (e) Close-up view of a white tuff bed (>2 m-thick) in a thin black shale layer in the DX C block.

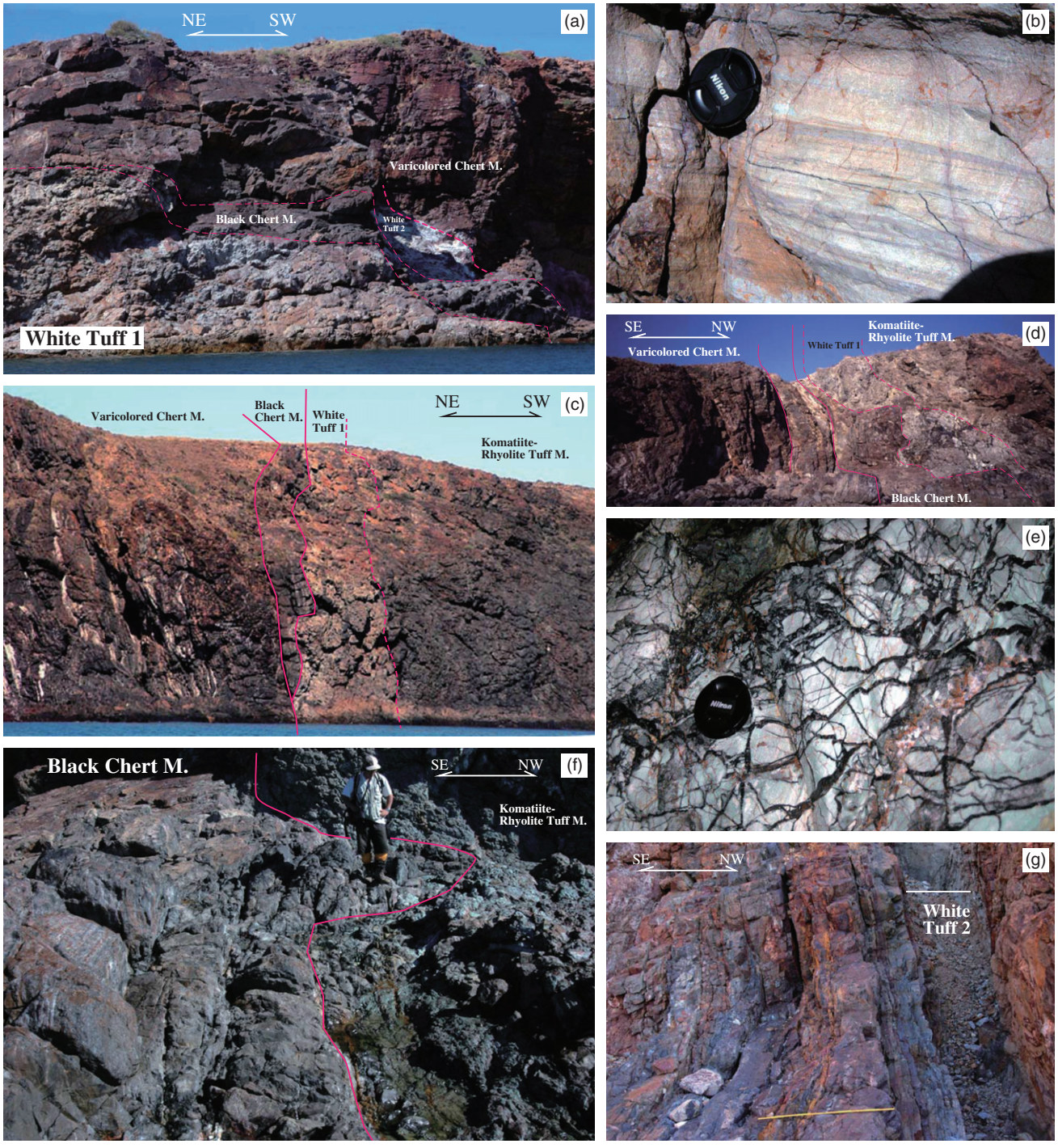


**Fig. 7** Characteristics of the DX D, DX E, and DX F blocks. (a) Overview of vertical bedding in the DX D block. White Tuff 1 is preserved along the cliff and reaches >9 m in thickness, but does not contain black chert veins. The Black Chert Member and White Tuff 2 occur to the right in the photograph. The hilltop consists of the Varicolored Chert Member. (b) Close-up view of well-laminated White Tuff 1 in the DX D block. This bed does not contain black chert veins. (c) Overview of a white tuff bed on the east side of the DX E block. White Tuff 1 and the Varicolored Chert Member are bounded by bedding-parallel strike-slip faults. White Tuff 1 is 9 m thick. The Black Chert Member and the Varicolored Chert Member are truncated by strike-slip faults. White Tuff 2 is partly preserved along this boundary. (d) Overview of the contact between the Black Chert and Varicolored Chert members on the east side of the DX F block. A highly altered zone cuts White Tuff 1 and the Black Chert Member. (e) Close-up view of White Tuff 1 in the DX F block. Web-like black chert veins cross-cut the thick white tuff. (f) Well-bedded greenish shale bed in the DX F block. Left side is the upper portion.

### DX D BLOCK

The DX D block, exposed for 150 m along the northern coast Dixon Island, is the smallest block on the island. The western part of the block contains well preserved and stratified Black Chert Member and White Tuff 2. The eastern part of the black chert and varicolored chert, where they meets the DX E block, is bounded by a highly weathered porphyry intrusion and a fault oriented subparallel to bedding.

This block is divided into east and west subdomains by a northwest–southeast-striking left-lateral fault oriented vertical and perpendicular to the strike of bedding which records an offset of more than 9 m. Consequently, the east subdomain contains the varicolored chert sequence and the west subdomain contains well-exposed White Tuff 1 and the black chert bed along the coast (Fig. 7). The fault is an early-stage normal fault ($F_0$) that post-dates the deposition of the Black Chert Member. A left-lateral $D_2$ strike-slip fault, which truncates the $F_0$ fault, occurs subparallel to bedding at the eastern margin of the block and contains pronounced striations on its fault plane, and is oriented vertically and parallel to the axes of asymmetric folds.

The east subdomain contains the well-preserved Black Chert Member (>8 m thick) that overlies White Tuff 1 and consists of massive and laminated black chert and highly silicified yellowish-brown biomat beds that resemble those preserved within black chert beds in the DX B and DX C blocks (Kiyokawa *et al.* 2006). White Tuff 2 also occurs in the east subdomain, and is cut by a $D_2$ strike-slip fault oriented subparallel to bedding.

In the east subdomain, well-preserved White Tuff 1 is 9 m thick and consists of massive, coarse-grained white tuff devoid of black chert veins (Fig. 7). The tuff bed is the thickest sequence on the island. The Black Chert Member does not occur in this subdomain because it is offset by a $D_2$ strike-slip fault.

### DX E BLOCK

The DX E block, which is 1200 m long where measured along the northern coast, is the longest block on Dixon Island (Fig. 3) and is characterized by continuous, 30–50 m-high cliffs of the Komatiite–Rhyolite Tuff Member. The eastern part of the block contains a stratified sequence comprising the Black Chert and Varicolored Chert members.

In the eastern part of the DX E block, White Tuff 1 (4–7 m thick) is exposed for over 70 m of horizontal distance along a hilltop above massive greenish siliceous tuff beds. The tuff bed is generally massive and is cut by black chert veins. The basal part of White Tuff 1 contains black chert breccia and is connected to felsic volcanic feeder dikes (2–3 m wide) that occur within silicified komatiite volcanic rocks of the Komatiite–Rhyolite Tuff Member. White Tuff 1 was supplied by these felsic feeder dikes in the ocean floor.

The well-stratified Black Chert Member is largely absent along the coastal outcrops of the DX E block due to deformation related to bedding-parallel strike-slip faults (Fig. 7). However, the member is exposed on nearby hilltops, where it is 3–4 m thick. Here, the member consists of several beds that contain aragonite with a fan texture (Kiyokawa *et al.* 2006), as well as black and white chert beds (10–20 cm thick) with aragonite–barite pseudomorphs after fibrous quartz.

White Tuff 2 occurs in a shear zone between bedded black chert beds and iron-bearing bedded chert beds. Its original thickness is difficult to estimate in this area because of the effects of strike-slip deformation.

The Varicolored Chert Member, which is well exposed along the coastline in the eastern part of the block, was folded into sigmoidal shapes about steep axes during left-lateral strike-slip $D_2$ deformation (Fig. 3). At the top of a coastal hill in the eastern part, this member is well preserved in continuous sections (Fig. 3), made up of very finely laminated chert and thin hematite-rich iron beds. A bedding-parallel porphyry intrusion is well preserved in the upper part of the sequence.

### DX F BLOCK

The DX F block, where exposed along the eastern coast of the island, contains a well-preserved stratigraphy (Figs 7,8). The Komatiite–Rhyolite Tuff Member exceeds 100 m in thickness and consists of highly altered, pale green volcanic rocks with numerous thin black chert veins. White Tuff 1, which occurs in the uppermost part of the altered volcanic zone, contains many black chert veins (Fig. 7e). The base of White Tuff 1 is difficult to distinguish because it is highly veined and altered where it overlies greenish volcanics. White Tuff 1 is overlain by a black chert bed along an irregular wavy contact with a relief of 0.5 to 1.0 m (Fig. 7f).

The Black Chert Member in the DX F block is 10 m thick, making it the thinnest black chert unit on Dixon Island. The member consists of laminated black chert beds and siliceous gray

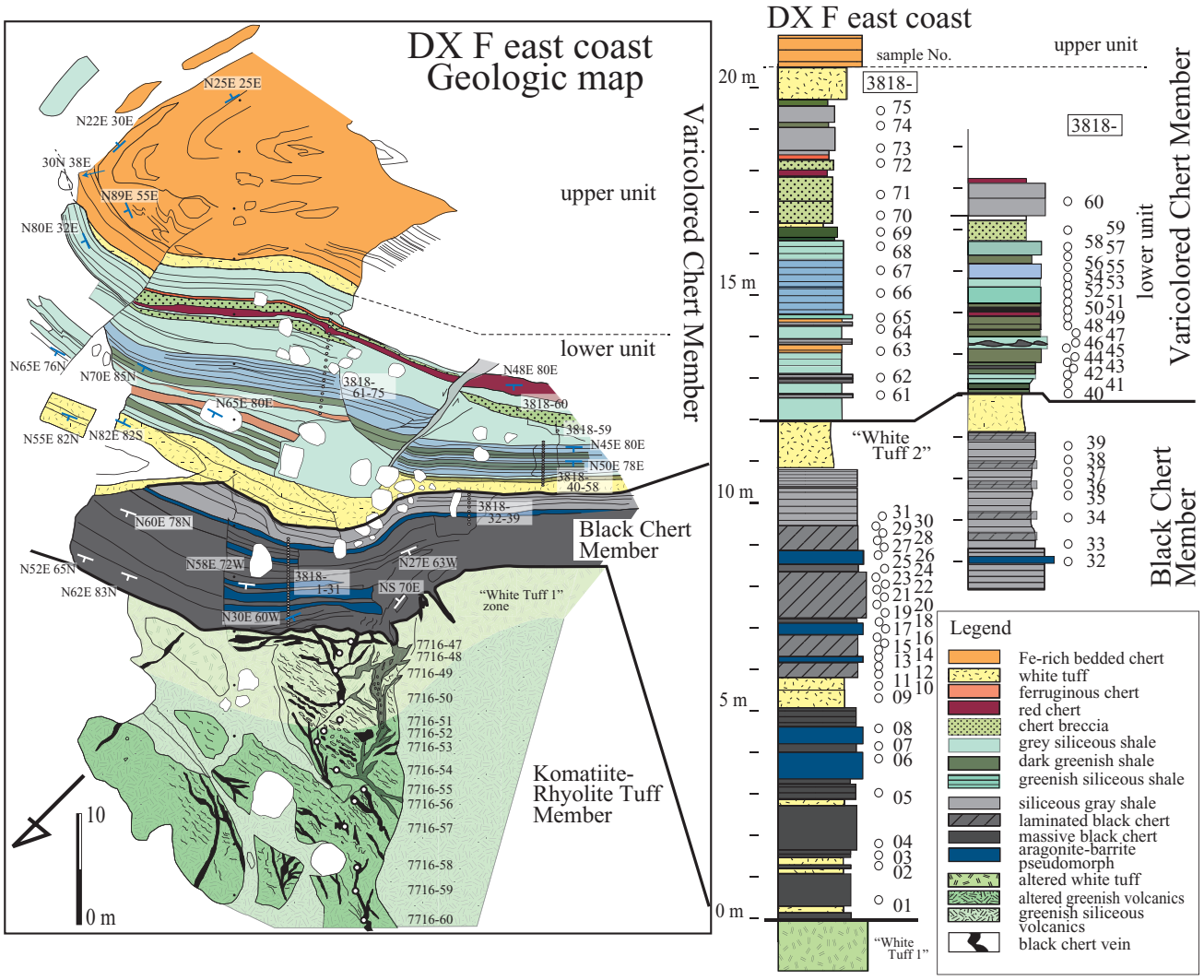


**Fig. 8** Geological map of the east side of the DX F block.

shale, along with several siliceous chert beds that contain aragonite–barite pseudomorphs after quartz. White Tuff 2 (50 cm thick) is strongly weathered and contains bedded shale exposed in a topographic depression (Fig. 7g).

The Varicolored Chert Member, which is better exposed here than in any other block, can be subdivided into two submembers: greenish chert and iron-rich chert. The lower submember consists of well-preserved, greenish bedded siliceous shale, dark greenish shale, and grey siliceous shale. The greenish bedded siliceous shale is massive and consists of clay minerals without quartz grains or organic matter. The upper unit consists of bedded chert and iron-rich chert beds. The eastern coast of the island, where the upper submember occurs, contains $D_1$-related map-scale folds with subhorizontal axes.

## LATERAL VARIATIONS IN THE STRATIGRAPHY OF THE DIXON ISLAND FORMATION

To document lateral variations in the paleoseafloor environment, it is important to identify key marker beds in each block that can be used to correlate lithologies and thicknesses between blocks. Based on the sedimentary characteristics observed along approximately 5 km of lateral stratigraphy, we recorded the distribution of white tuff beds as key marker beds, thickness changes of the Black Chert Member, and the distribution of hydrothermal alteration within the uppermost part of the Komatiite–Rhyolite Tuff Member.

White Tuff 1 and White Tuff 2 occur as well-stratified tuff beds in the uppermost parts of the Komatiite–Rhyolite Tuff Member and the Black Chert Member, respectively. White Tuff 1 is

medium- to coarse-grained felsic tuff that occurs as well-stratified beds. The thickness of the tuff varies among the blocks, from a maximum of 9 m in the DX D block to 4–7 m in the eastern part of the DX E block, and 1.5–2.0 m in the DX B and DX C blocks.

White Tuff 2 consists of finely laminated white felsic tuff and thin gray-black shale. This generally soft, weathered tuff forms topographic depressions and is locally deformed by strike-slip faults. Less-deformed sections (>3 m thick) are preserved in the DX C and DX D blocks, whereas the tuff is <1.0 m thick in the DX A and DX F blocks.

The Black Chert Member varies in thickness from 20 m in the DX B block to <10 m in the DX A, DX E, and DX F blocks. The thicknesses of White Tuff 1 and 2, and the total thickness of the Black Chert Member, reflect minor topographic variations in the paleo-seafloor. Thicker tuff beds may represent particulate flow deposits that accumulated in small depressions on the paleo-seafloor.

White Tuff 1 contains localized zones of hydrothermal alteration. Variations in the thickness of White Tuff 1 indicate that it is locally disrupted or absent due to intensive alteration and veining within the black chert at the contact with the Komatiite–Rhyolite Tuff Member. The upper and lower contacts of White Tuff 1 in the DX C, DX E, and DX F blocks are obscured by hydrothermal alteration, making it difficult to accurately measure its thickness.

Localized areas of intense hydrothermal alteration in the uppermost part of the Komatiite–Rhyolite Tuff Member indicate that hydrothermal circulation or hydrothermal vent systems had a patchy distribution and were spaced at minimum intervals of several hundred meters on the paleo-ocean floor. At the sites of vent systems on the ocean floor, the Komatiite–Rhyolite Tuff Member was intruded by black chert veins that contain organic carbon; the veins terminate at the bottom of the thick black chert bed. This observation indicates that most of the hydrothermal low-temperature fluid seeped to the ocean surface through the black chert vein systems, most of which are overlain by organic-rich cherty sediments.

Alteration zones in coarse-grained komatiite beds of the Komatiite–Rhyolite Tuff Member are relatively intensive and continuous. These zones are thought to have resulted from a >5 km-wide zone of hydrothermal circulation. The black chert veins and early-stage quartz-rich veins may also be related to these altered zones.

## LATERAL VARIATIONS IN THE DISTRIBUTION OF ORGANIC CARBON

The organic-carbon-bearing black chert sequence, which is mainly represented by the Black Chert Member of the Dixon Island Formation, is inferred to record organic activity in the ocean during its formation in the Mesoarchean. The lateral thickness changes and stratigraphic variations of the black chert sequence in each block were controlled by the activity of low-temperature organic-rich hydrothermal venting that occurred through the black chert veins. The preferred orientations of these veins indicate their geometry was controlled by the paleo-stress field (Kiyokawa & Taira 1998). Weak, low-temperature, organic-matter-bearing hydrothermal activity may have occurred in the water column, and large amounts of organic matter precipitated around hydrothermal vents. Spatial variations in the amount of organic carbon may have resulted from local biological activity within hydrothermal vent systems. In particular, the $C_{org}$ contents and carbon isotopes compositions ($\delta^{13}C_{org}$) show stratigraphic and lateral variations within the sedimentary sequence, which could be related to differences in the activity and origins of organic matter in the black chert. These data provide a proxy for lateral changes in hydrothermal and biological activity on the paleo-ocean floor.

### METHODS

To document stratigraphic variations and lateral carbon variations, samples of black chert, red chert, greenish shale, and black chert veins were collected from fresh continuous outcrops in each block where detailed stratigraphic columns could be measured (Fig. 5).

Powdered samples were treated with 3 M HCl in a silver cup at room temperature for 2 days to remove the carbonate fraction. Residual samples were analyzed for $C_{org}$ content and carbon isotope compositions using an elemental analyzer (FlashEA 1112; Bath, UK) coupled to a Delta-Plus Advantage (ThermoFinnigan; Ringoes, NJ, USA) isotope ratio mass spectrometer (EA-IRMS) at Kochi University, Japan. The analytical uncertainty for the determination of $C_{org}$ content by this method was within 0.01 wt%. The precision for $\delta^{13}C_{org}$ determinations was better than 0.1‰.

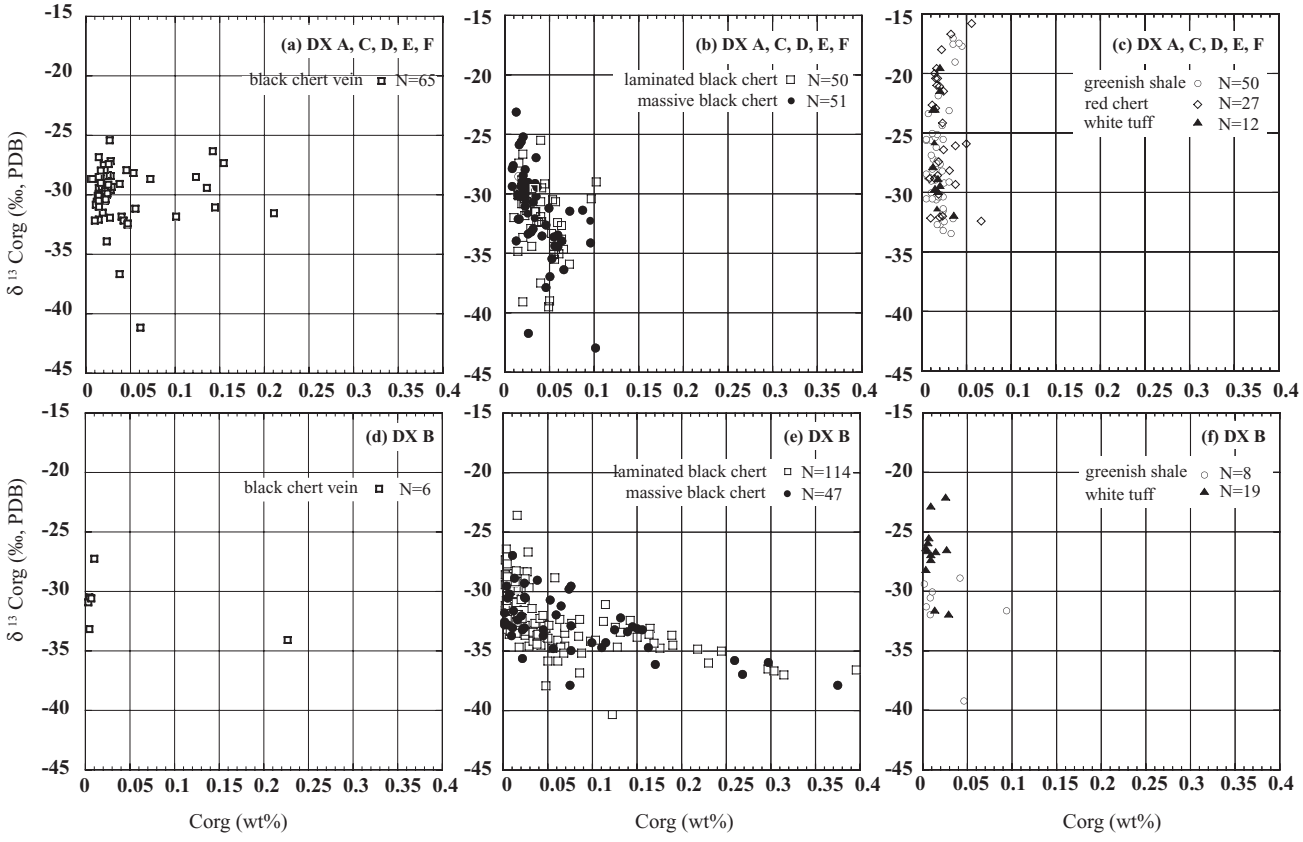


**Fig. 9** Lateral variations in the organic carbon ($C_{org}$) contents and carbon isotope compositions ($\delta^{13}C_{org}$). Data from the DX B block are after Ikehara *et al.* (unpubl. data, 2012). PDB, Peedee belemnite.

## CONTENTS AND ISOTOPE COMPOSITIONS OF ORGANIC CARBON

The patterns of lithological and lateral stratigraphic variations in the $C_{org}$ contents and $\delta^{13}C_{org}$ values are shown in Figures 9 and 10; the raw data are listed in Table 2. Lithological classification is based on plots of $\delta^{13}C_{org}$ versus $C_{org}$ (Fig. 9). Lateral variations in stratigraphy are shown in two groups based on the proportion of organic-rich rocks: (i) the DX A, DX C, DX D, and DX E blocks; and (ii) the DX F and DX B blocks (this latter group contains a high proportion of organic-rich rocks). Data for the DX B block are partly from Kiyokawa *et al.* (2006).

## LITHOLOGICAL CLASSIFICATION

Three rock types were examined to assess the nature of lateral variations in stratigraphy in the organic carbon signature: black chert veins, laminated and massive black chert, and other rocks (greenish shale, red chert, and white tuff). The black chert veins yielded $C_{org} < 0.2$ wt% and $\delta^{13}C_{org}$ values of –33 to –27‰, with the lowest $\delta^{13}C_{org}$ value of –42‰.

In comparison, samples of laminated and massive black chert in the DX A, DX C, DX D, DX E, and DX F blocks yield lower $C_{org}$ values of <0.1 wt% and similar $\delta^{13}C_{org}$ values of –39 to –23‰, although several samples have values of –43 to –40‰. The $C_{org}$ contents of the DX B block are much higher than those of the other blocks, which have maximum values of 0.4 wt%. Samples of other rock types (greenish shale, red chert, and white tuff) typically yield very low $C_{org}$ contents (<0.4 wt%) and $\delta^{13}C_{org}$ values of –30 to –15‰.

## LATERAL VARIATIONS IN STRATIGRAPHY

The black chert veins in each block contain 0.02–0.14 wt% organic carbon and show no lateral (or depth) variations. The lower parts of the Black Chert Member in the DX A, DX B, and DX D blocks clearly have higher values of $C_{org}$ than the upper parts. However, the DX C block contains higher $C_{org}$ contents in the upper part of the Black Chert Member than in the lower part. The lower

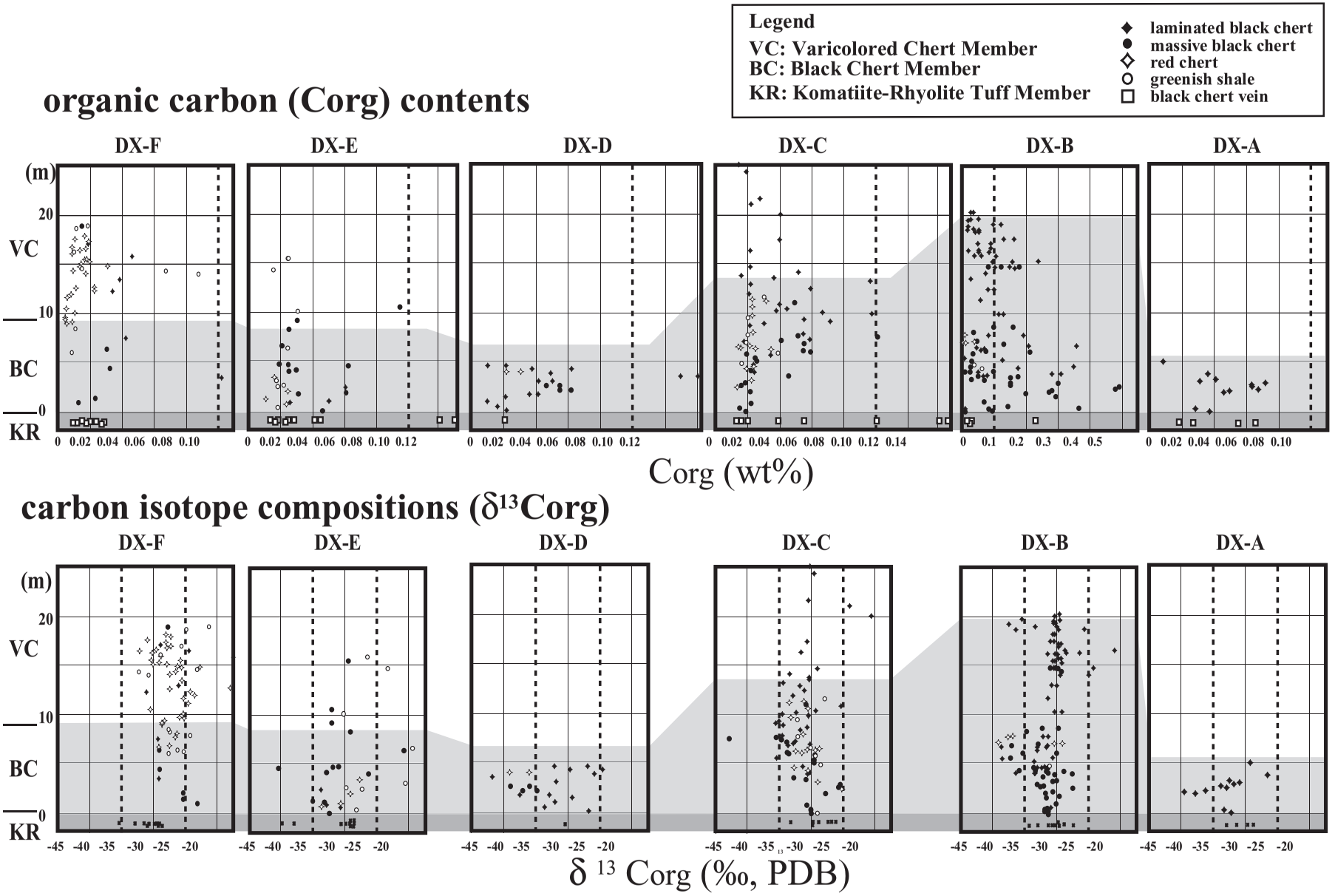


**Fig. 10** Lithological variations in the organic carbon ($C_{org}$) contents and carbon isotope compositions ($\delta^{13}C_{org}$) for black chert veins, laminated black chert, massive black chert, and other sediments with low concentrations of organic matter. Vertical axis shows the stratigraphic subdivision and gray shading indicates the Black Chert (BC) and Komatiite–Rhyolite Tuff (KR) Members. VC, Varicolored Chert Member.

**Table 2** Organic carbon ($C_{org}$) contents and carbon isotope values ($\delta^{13}C_{org}$) for black chert and black chert veins in all blocks

| No. | Sample ID | Area | Lithology | $C_{org}$ (wt%) | $\delta^{13}C_{org}$(‰) |
|---|---|---|---|---|---|
| 1 | 5813-01 | DX A | Laminated black chert | 0.04 | –32.32 |
| 2 | 5813-02 | DX A | Massive black chert | 0.03 | –33.21 |
| 3 | 5813-03 | DX A | Massive black chert | 0.05 | –37.85 |
| 4 | 5813-04 | DX A | Laminated black chert (weakly) | 0.05 | –39.49 |
| 5 | 5813-05 | DX A | Massive black chert (with thin lamination) | 0.07 | –36.34 |
| 6 | 5813-06 | DX A | Laminated black chert | 0.06 | –32.69 |
| 7 | 5813-07 | DX A | Massive black chert | 0.06 | –33.93 |
| 8 | 5813-08 | DX A | Massive black chert | 0.07 | –31.38 |
| 9 | 5813-09 | DX A | Massive black chert | 0.03 | –30.74 |
| 10 | 5813-10 | DX A | Laminated black chert with white tuff | 0.04 | –32.34 |
| 11 | 5813-11 | DX A | Massive black chert with breccia | 0.03 | –26.95 |
| 12 | 5813-12 | DX A | Massive black chert with breccia | 0.04 | –29.42 |
| 13 | 5813-13 | DX A | White tuff/black chert fragment (sst) | 0.02 | –21.43 |
| 14 | 5813-14 | DX A | Massive black chert with breccia | 0.01 | –29.29 |
| 15 | 5813-17 | DX A | Massive black chert | 0.01 | –33.92 |
| 16 | 5813-18 | DX A | Massive black chert | 0.02 | –32.06 |
| 17 | 5813-19 | DX A | Laminated black chert | 0.01 | –34.81 |
| 18 | 5813-20 | DX A | Laminated black chert | 0.02 | –30.78 |
| 19 | 5813-21 | DX A | White tuff conglomerate | 0.02 | –28.84 |
| 20 | 7718-16 | DX A | Black chert vein | 0.07 | –28.67 |
| 21 | 7718-17 | DX A | Black chert vein | 0.06 | –31.16 |
| 22 | 7718-18 | DX A | Black chert vein | 0.02 | –29.92 |
| 23 | 7718-19 | DX A | Black chert vein | 0.03 | –28.41 |
| 24 | 7718-20 | DX A | Black chert vein | 0.02 | –30.07 |
| 25 | 7718-10 | DX B west | Black chert vein | 0.02 | –28.24 |
| 26 | 7718-14 | DX B west | Black chert vein | 0.01 | –30.31 |
| 27 | 7718-15 | DX B west | Black chert vein | 0.02 | –29.73 |
| 28 | 1007-02 | DX C | Black chert vein | 0.01 | –28.50 |
| 29 | 1007-04 | DX C | White tuff | 0.01 | –29.90 |
| 30 | 1007-06 | DX C | Black chert vein upper | 0.03 | –30.28 |
| 31 | 1009-08 | DX C | Massive black chert in tuff worm | 0.03 | –26.72 |
| 32 | 1009-09 | DX C | Massive black chert in tuff worm | 0.01 | –30.41 |
| 33 | 1009-11 | DX C | Massive gray chert with white tuff | 0.01 | –31.78 |
| 34 | 1009-16 | DX C | White tuff glass | 0.01 | –33.60 |
| 35 | 1009-18 | DX C | Massive black chert upper (7.2 m) | 0.01 | –33.71 |
| 36 | 1009-19 | DX C | Massive black chert (7.4 m) | 0.02 | –31.76 |
| 37 | 1009-21 | DX C | Laminated black chert | 0.04 | –28.58 |
| 38 | 5817-100 | DX C | Greenish chert | 0.02 | –32.68 |
| 39 | 5817-101 | DX C | Laminated black chert | 0.06 | –30.71 |
| 40 | 5817-102 | DX C | Massive black chert with breccia | 0.06 | –34.38 |
| 41 | 5817-103 | DX C | Greenish chert | 0.02 | –31.83 |
| 42 | 5817-104 | DX C | Massive black chert | 0.10 | –34.14 |
| 43 | 5817-105 | DX C | Massive black chert | 0.04 | –30.19 |
| 44 | 5817-106 | DX C | Laminated black chert | 0.02 | –30.16 |
| 45 | 5817-107 | DX C | Laminated black chert | 0.05 | –33.30 |
| 46 | 5817-108 | DX C | Laminated black chert | 0.02 | –29.11 |
| 47 | 5817-109 | DX C | Laminated black chert | 0.02 | –31.76 |
| 48 | 5817-110 | DX C | Laminated black chert | 0.04 | –30.67 |
| 49 | 5817-111 | DX C | Laminated black chert | b.d. | n.a. |
| 50 | 5817-112 | DX C | Red Fe-rich/laminated black chert | 0.02 | –24.18 |
| 51 | 5817-112 | DX C | Laminated black chert | b.d. | n.a. |
| 52 | 5817-113 | DX C | Laminated black chert | 0.03 | –30.34 |
| 53 | 5817-113 | DX C | Laminated black chert | b.d. | n.a. |
| 54 | 5817-114 | DX C | Laminated black chert | 0.02 | –29.70 |
| 55 | 5817-114 | DX C | Laminated black chert | b.d. | n.a. |
| 56 | 5817-115 | DX C | Laminated black chert | 0.01 | –30.07 |
| 57 | 5817-115 | DX C | Laminated black chert | b.d. | n.a. |
| 58 | 5817-116 | DX C | Massive black chert | 0.02 | –30.03 |
| 59 | 5817-116 | DX C | Massive black chert | b.d. | n.a. |
| 60 | 5817-117 | DX C | White tuff | 0.02 | –29.73 |
| 61 | 5817-117 | DX C | White tuff | b.d. | n.a. |
| 62 | 5817-118 | DX C | White tuff | 0.02 | –29.87 |
| 63 | 5817-118 | DX C | White tuff | b.d. | n.a. |
| 64 | 5817-119 | DX C | Red chert | b.d. | n.a. |

**Table 2** *Continued*

| No. | Sample ID | Area | Lithology | $C_{org}$ (wt%) | $\delta^{13}C_{org}$(‰) |
|---|---|---|---|---|---|
| 65 | 5817-119 | DX C | Red chert | b.d. | n.a. |
| 66 | 5817-120 | DX C | Massive black chert | 0.01 | –30.09 |
| 67 | 5817-120 | DX C | Massive black chert | b.d. | n.a. |
| 68 | 5817-121 | DX C | Massive black chert | 0.02 | –30.98 |
| 69 | 5817-121 | DX C | Massive black chert | b.d. | n.a. |
| 70 | 5817-44 | DX C | Massive black chert | 0.02 | –27.86 |
| 71 | 5817-45 | DX C | Greenish chert | 0.01 | –25.13 |
| 72 | 5817-46 | DX C | Massive black chert | 0.02 | –25.83 |
| 73 | 5817-47 | DX C | Massive black chert | 0.02 | –25.58 |
| 74 | 5817-48 | DX C | Greenish chert | 0.02 | –28.20 |
| 75 | 5817-49 | DX C | Massive black chert | b.d. | n.a. |
| 76 | 5817-50 | DX C | Massive black chert | 0.05 | –32.62 |
| 77 | 5817-51 | DX C | White tuff | 0.01 | –22.98 |
| 78 | 5817-52 | DX C | Laminated black chert | 0.03 | –30.67 |
| 79 | 5817-53 | DX C | Massive black chert | 0.02 | –30.27 |
| 80 | 5817-54 | DX C | Greenish chert | 0.02 | –30.37 |
| 81 | 5817-55 | DX C | Greenish chert | 0.02 | –32.36 |
| 82 | 5817-56 | DX C | Laminated black chert | 0.02 | –31.37 |
| 83 | 5817-57 | DX C | Red chert | 0.02 | –28.83 |
| 84 | 5817-58 | DX C | Massive black chert | 0.02 | –29.73 |
| 85 | 5817-59 | DX C | Massive black chert barite pseudomorph | 0.03 | –28.95 |
| 86 | 5817-60 | DX C | Laminated black chert | 0.06 | –35.53 |
| 87 | 5817-61 | DX C | Laminated black chert | 0.03 | –31.52 |
| 88 | 5817-62 | DX C | Massive black chert barite pseudomorph | 0.02 | –29.31 |
| 89 | 5817-63 | DX C | Red chert | 0.04 | –29.27 |
| 90 | 5817-64 | DX C | Massive black chert barite pseudomorph | 0.06 | –33.37 |
| 91 | 5817-65 | DX C | Massive black chert | 0.05 | –33.63 |
| 92 | 5817-66 | DX C | Greenish chert | 0.03 | –32.16 |
| 93 | 5817-67 | DX C | Greenish chert | 0.03 | –29.20 |
| 94 | 5817-68 | DX C | Greenish chert | 0.02 | –30.60 |
| 95 | 5817-69 | DX C | Greenish chert | 0.01 | –28.94 |
| 96 | 5817-70 | DX C | Greenish chert | 0.02 | –30.20 |
| 97 | 5817-71 | DX C | Massive black chert | 0.06 | –34.28 |
| 98 | 5817-72 | DX C | Red chert | 0.02 | –30.22 |
| 99 | 5817-73 | DX C | Greenish chert | 0.02 | –32.66 |
| 100 | 5817-74 | DX C | Massive black chert | 0.04 | –33.48 |
| 101 | 5817-75 | DX C | Laminated black chert | 0.06 | –32.36 |
| 102 | 5817-76 | DX C | Red chert | b.d. | |
| 103 | 5817-77 | DX C | Massive black chert | 0.10 | –42.94 |
| 104 | 5817-78 | DX C | Massive black chert | 0.05 | –35.40 |
| 105 | 5817-79 | DX C | Red chert | 0.02 | –32.11 |
| 106 | 5817-80 | DX C | Laminated black chert | 0.05 | –34.44 |
| 107 | 5817-81 | DX C | Greenish chert | 0.02 | –31.49 |
| 108 | 5817-83 | DX C | Laminated black chert | b.d. | |
| 109 | 5817-84 | DX C | Laminated black chert | 0.02 | –30.44 |
| 110 | 5817-85 | DX C | Laminated black chert | 0.03 | –34.41 |
| 111 | 5817-86 | DX C | Laminated black chert | 0.07 | –35.94 |
| 112 | 5817-87 | DX C | Laminated black chert | 0.06 | –35.06 |
| 113 | 5817-88 | DX C | Red chert (laminated) | 0.02 | –31.96 |
| 114 | 5817-89 | DX C | Greenish chert | 0.02 | –33.25 |
| 115 | 5817-90 | DX C | Laminated black chert | 0.10 | –30.39 |
| 116 | 5817-91 | DX C | Laminated black chert | 0.07 | –34.68 |
| 117 | 5817-92 | DX C | Laminated black chert | 0.04 | –32.39 |
| 118 | 5817-93 | DX C | Laminated black chert | 0.04 | –29.15 |
| 119 | 5817-94 | DX C | Greenish chert | 0.02 | –30.29 |
| 120 | 5817-95 | DX C | Laminated black chert | 0.04 | –25.46 |
| 121 | 5817-96 | DX C | Massive black chert | 0.05 | –31.15 |
| 122 | 5817-97 | DX C | Greenish chert | 0.03 | –33.44 |
| 123 | 5817-98 | DX C | Greenish chert | 0.02 | –31.29 |
| 124 | 5817-99 | DX C | Red chert | 0.03 | –28.24 |
| 125 | 7717-25 | DX C | Black chert vein | 0.10 | –31.78 |
| 126 | 7717-26 | DX C | Black chert vein | 0.05 | –28.19 |
| 127 | 7717-27 | DX C | Black chert vein | 0.15 | –27.28 |
| 128 | 7717-28 | DX C | Black chert vein | 0.14 | –26.33 |

**Table 2** *Continued*

| No. | Sample ID | Area | Lithology | $C_{org}$ (wt%) | $\delta^{13}C_{org}$(‰) |
|---|---|---|---|---|---|
| 129 | 7717-30 | DX C | Black chert vein | 0.04 | –36.75 |
| 130 | 7717-31 | DX C | Black chert vein | 0.02 | –29.93 |
| 131 | 7717-32 | DX C | Black chert vein | 0.01 | –30.13 |
| 132 | 7717-33 | DX C | Black chert vein | 0.01 | –31.00 |
| 133 | 3820-01 | DX D | Laminated black chert | 0.02 | –26.74 |
| 134 | 3820-02 | DX D | Laminated black chert | 0.02 | –33.68 |
| 135 | 3820-03 | DX D | Laminated black chert (weakly) | 0.01 | –31.97 |
| 136 | 3820-05 | DX D | Laminated black chert | 0.02 | –29.24 |
| 137 | 3820-06 | DX D | Laminated black chert | 0.04 | –37.45 |
| 138 | 3820-07 | DX D | Massive black chert | 0.05 | –36.91 |
| 139 | 3820-08 | DX D | Laminated black chert (weakly) | 0.05 | –39.00 |
| 140 | 3820-09 | DX D | Laminated black chert | 0.04 | –31.86 |
| 141 | 3820-10 | DX D | Massive black chert (breccia) | 0.02 | –25.15 |
| 142 | 3820-11 | DX D | Massive black chert (breccia) | b.d. | n.a. |
| 143 | 3820-12 | DX D | Laminated black chert | 0.13 | –45.12 |
| 144 | 3820-13 | DX D | Red Fe rich/laminated black chert | 0.05 | –25.86 |
| 145 | 3820-14 | DX D | Laminated gray shale | 0.02 | –39.07 |
| 146 | 3820-16 | DX D | Red chert (laminated) | 0.01 | –32.21 |
| 147 | 7717-09 | DX D | Black chert vein | 0.02 | –30.45 |
| 148 | 3815-01 | DX E | Black chert vein | 0.02 | –31.49 |
| 149 | 3815-02 | DX E | Black chert vein | 0.04 | –31.79 |
| 150 | 3815-03 | DX E | Black chert vein | 0.02 | –29.71 |
| 151 | 3815-04 | DX E | Black chert vein in white tuff | 0.02 | –33.88 |
| 152 | 3815-05 | DX E | Black chert vein in white tuff | 0.06 | –41.19 |
| 153 | 3815-06 | DX E | White chert (barite pseudomorph) | 0.04 | –31.87 |
| 154 | 3815-07 | DX E | White tuff (white) | 0.01 | –23.05 |
| 155 | 3815-10 | DX E | Black chert vein/red chert | 0.02 | –29.29 |
| 156 | 3815-11 | DX E | Black chert vein/red chert | 0.02 | –29.92 |
| 157 | 3815-12 | DX E | Greenish chert | 0.01 | –27.83 |
| 158 | 3815-13 | DX E | Massive black chert | 0.03 | –33.34 |
| 159 | 3815-14 | DX E | Red- black chert(long fault) | 0.02 | –26.43 |
| 160 | 3815-15 | DX E | Black chert vein top | 0.05 | –32.53 |
| 161 | 3815-16 | DX E | Red chert (laminated) | 0.02 | –28.63 |
| 162 | 3815-17 | DX E | Laminated black chert | 0.05 | –30.47 |
| 163 | 3815-18 | DX E | Massive black chert | 0.02 | –28.78 |
| 164 | 3815-19 | DX E | Massive black chert | 0.03 | –32.92 |
| 165 | 3815-20 | DX E | Red chert (with black chert breccia) | 0.02 | –27.43 |
| 166 | 3815-21 | DX E | Red Fe rich/laminated black chert | 0.02 | –20.40 |
| 167 | 3815-22 | DX E | Laminated black chert | 0.03 | –32.86 |
| 168 | 3815-23 | DX E | Laminated black chert fine sandstone layer) | 0.02 | –30.76 |
| 169 | 3815-24 | DX E | Red chert (massive) | 0.02 | –21.47 |
| 170 | 3815-25 | DX E | White tuff (white-red) | 0.02 | –19.55 |
| 171 | 3816-01A | DX E | Black chert vein in komatiite | 0.21 | –31.68 |
| 172 | 3816-01B | DX E | Black chert vein (breccia) | 0.14 | –31.16 |
| 173 | 3816-02 | DX E | Black chert vein type 2 | 0.02 | –28.09 |
| 174 | 3816-03 | DX E | Greenish altered volcanics (komatiite) | b.d. | –17.96 |
| 175 | 3816-04A | DX E | Black chert vein (jasper) | b.d. | –21.52 |
| 176 | 3816-04B | DX E | Quartz vein (first)/red chert | 0.07 | –14.12 |
| 177 | 3816-05A | DX E | Black chert vein | 0.01 | –31.17 |
| 178 | 3816-05B | DX E | Black chert vein | 0.02 | –30.12 |
| 179 | 3816-06 | DX E | Black chert vein | 0.05 | –27.98 |
| 180 | 3816-07 | DX E | Black chert vein (breccia) type 1 | 0.02 | –29.96 |
| 181 | 3816-08 | DX E | Black chert vein type 1 | 0.02 | –30.53 |
| 182 | 3816-09 | DX E | Black chert vein | | –30.03 |
| 183 | 3816-10 | DX E | Massive black chert | 0.02 | –29.54 |
| 184 | 3817-01 | DX E | White tuff (felsic) | 0.02 | –31.26 |
| 185 | 3817-02 | DX E | Black chert vein/quartz vein | 0.03 | –32.03 |
| 186 | 3817-03 | DX E | Massive black chert breccia/felsic tuff | 0.02 | –31.99 |
| 187 | 3817-04 | DX E | Laminated black chert | 0.06 | –33.57 |
| 188 | 3817-05 | DX E | Laminated black chert | 0.06 | –35.01 |
| 189 | 3817-06 | DX E | Greenish chert | 0.01 | –30.66 |
| 190 | 3817-08 | DX E | Massive black chert/quartz vein | 0.03 | –29.02 |
| 191 | 3817-09 | DX E | Massive black chert | 0.03 | –32.22 |
| 192 | 3817-10 | DX E | Laminated gray chert (felsic tuff) | 0.03 | –30.15 |

**Table 2** *Continued*

| No. | Sample ID | Area | Lithology | $C_{org}$ (wt%) | $\delta^{13}C_{org}$(‰) |
|---|---|---|---|---|---|
| 193 | 3817-11 | DX E | Massive black chert | 0.09 | –32.35 |
| 194 | 3817-13 | DX E | White tuff (felsic) | 0.02 | –25.55 |
| 195 | 3817-15 | DX E | Red chert | 0.02 | –23.36 |
| 196 | 3817-16 | DX E | Greenish gray chert (breccia) | 0.03 | –26.74 |
| 197 | 3817-17 | DX E | Laminated black chert | 0.03 | –29.49 |
| 198 | 3817-18 | DX E | Greenish gray chert | 0.02 | –17.95 |
| 199 | 3817-19 | DX E | Laminated black chert | 0.03 | –16.73 |
| 200 | 3817-20 | DX E | Laminated black chert/felsic tuff | 0.03 | –20.78 |
| 201 | 3817-21 | DX E | Laminated black chert/felsic tuff | 0.06 | –15.53 |
| 202 | 7717-10 | DX E west coast | Black chert vein | 0.02 | –28.31 |
| 203 | 7717-11 | DX E west coast | Black chert vein | 0.03 | –27.19 |
| 204 | 7717-12 | DX E west coast | Black chert vein | 0.01 | –29.42 |
| 205 | 7717-15 | DX E west coast | Black chert vein | 0.12 | –28.47 |
| 206 | 7717-16 | DX E west mid hill | Black chert vein | 0.04 | –32.22 |
| 207 | 7717-17 | DX E west mid hill | Black chert vein | 0.03 | –29.58 |
| 208 | 7717-18 | DX E west mid hill | Black chert vein | 0.02 | |
| 209 | 7717-19 | DX E west mid hill | Black chert vein | 0.02 | –30.03 |
| 210 | 7717-20 | DX E west mid hill | Black chert vein | 0.01 | –30.59 |
| 211 | 7717-21 | DX E west mid hill | Black chert vein | 0.01 | –30.94 |
| 212 | 7717-22 | DX E west mid hill | Black chert vein | 0.01 | –30.50 |
| 213 | 7717-23 | DX E west mid hill | Black chert vein | 0.04 | –29.14 |
| 214 | 7717-24 | DX E west mid hill | Black chert vein | 0.14 | –29.43 |
| 215 | 3818-01 | DX F | Massive black chert/quartz vein | 0.01 | –23.07 |
| 216 | 3818-02 | DX F | Greenish gray chert (tuff) | 0.02 | –25.51 |
| 217 | 3818-03 | DX F | Massive black chert | b.d. | n.a. |
| 218 | 3818-05 | DX F | Laminated black chert | 0.10 | –29.01 |
| 219 | 3818-07 | DX F | Massive black chert | 0.03 | –29.07 |
| 220 | 3818-09 | DX F | White tuff (white) | 0.01 | –27.79 |
| 221 | 3818-10 | DX F | White tuff breccia (quartz vein) | 0.02 | –29.43 |
| 222 | 3818-11 | DX F | Massive black chert | 0.01 | –27.78 |
| 223 | 3818-12 | DX F | Greenish shale (massive) | b.d. | n.a. |
| 224 | 3818-13 | DX F | Greenish shale (massive) | 0.03 | –29.10 |
| 225 | 3818-14 | DX F | Greenish shale (massive) | b.d. | n.a. |
| 226 | 3818-15 | DX F | Massive black chert | b.d. | n.a. |
| 227 | 3818-16 | DX F | Greenish chert | b.d. | n.a. |
| 228 | 3818-18 | DX F | Greenish shale (massive) | 0.01 | –28.99 |
| 229 | 3818-20 | DX F | Laminated black/red chert | 0.04 | –29.52 |
| 230 | 3818-21 | DX F | Laminated black chert | b.d. | n.a. |
| 231 | 3818-22 | DX F | Laminated black chert | b.d. | n.a. |
| 232 | 3818-24 | DX F | Laminated black chert | b.d. | n.a. |
| 233 | 3818-25 | DX F | Greenish gray chert (breccia) | 0.01 | –27.99 |
| 234 | 3818-26 | DX F | Red chert (breccia) | b.d. | n.a. |
| 235 | 3818-27 | DX F | Greenish shale (massive) | 0.01 | –28.74 |
| 236 | 3818-28 | DX F | Greenish shale (massive) | 0.01 | –28.69 |
| 237 | 3818-29 | DX F | Greenish shale (massive) | 0.00 | –28.38 |
| 238 | 3818-30 | DX F | Greenish shale (massive) | 0.00 | –25.56 |
| 239 | 3818-31 | DX F | Greenish chert | 0.01 | –25.64 |
| 240 | 3818-32 | DX F | Red chert | b.d. | n.a. |
| 241 | 3818-33 | DX F | Greenish chert | 0.00 | –30.52 |
| 242 | 3818-34 | DX F | Greenish shale (massive) | b.d. | n.a. |
| 243 | 3818-35 | DX F | Greenish shale (massive) | 0.01 | –25.54 |
| 244 | 3818-36 | DX F | Greenish shale (massive) | 0.01 | –23.26 |
| 245 | 3818-37 | DX F | Greenish shale (massive) | 0.02 | –24.33 |
| 246 | 3818-38 | DX F | Greenish chert | 0.01 | –27.18 |
| 247 | 3818-39 | DX F | Greenish shale (massive) | b.d. | n.a. |
| 248 | 3818-40 | DX F | Greenish chert | 0.02 | –27.33 |
| 249 | 3818-41 | DX F | Greenish chert | 0.01 | –26.76 |
| 250 | 3818-42 | DX F | Red chert (laminated) Fe rich | 0.02 | –22.89 |
| 251 | 3818-43 | DX F | Greenish chert | 0.01 | –25.29 |
| 252 | 3818-44 | DX F | Greenish chert (weakly) | b.d. | n.a. |
| 253 | 3818-45 | DX F | Red chert with quartz vein | b.d. | n.a. |
| 254 | 3818-46 | DX F | Massive black chert (fragment) | 0.02 | –28.41 |
| 255 | 3818-47 | DX F | Greenish shale (massive) | 0.02 | –30.33 |
| 256 | 3818-49 | DX F | Greenish shale (massive) | b.d. | n.a. |

**Table 2** *Continued*

| No. | Sample ID | Area | Lithology | $C_{org}$ (wt%) | $\delta^{13}C_{org}$(‰) |
|---|---|---|---|---|---|
| 257 | 3818-50 | DX F | Red chert (laminated Fe rich) | 0.01 | –28.80 |
| 258 | 3818-51 | DX F | Greenish shale (massive) | 0.01 | –29.96 |
| 259 | 3818-52 | DX F | Massive black chert | 0.01 | –32.14 |
| 260 | 3818-53 | DX F | Massive black chert | 0.02 | –29.33 |
| 261 | 3818-54 | DX F | Massive gray chert | 0.01 | –27.64 |
| 262 | 3818-55 | DX F | Massive gray chert | b.d. | n.a. |
| 263 | 3818-56 | DX F | Laminated black chert | 0.02 | –28.82 |
| 264 | 3818-57 | DX F | Greenish shale (massive) | 0.02 | –27.55 |
| 265 | 3818-58 | DX F | Greenish shale (massive) | 0.01 | –30.50 |
| 266 | 3818-59 | DX F | Greenish chert (sandy) | b.d. | n.a. |
| 267 | 3818-60 | DX F | Laminated black chert | 0.02 | –27.40 |
| 268 | 3818-61 | DX F | Laminated black chert | 0.03 | –31.47 |
| 269 | 3818-62 | DX F | Red Fe rich/laminated black chert | 0.02 | –18.02 |
| 270 | 3818-62A | DX F | Red Fe rich/laminated black chert | 0.02 | –21.14 |
| 271 | 3818-62B | DX F | Red chert/laminated black chert | 0.02 | –20.04 |
| 272 | 3818-62C | DX F | Red chert/laminated black chert | 0.02 | –19.61 |
| 273 | 3818-62D | DX F | Red chert/laminated black chert | 0.02 | –20.42 |
| 274 | 3818-63 | DX F | Red Fe rich/laminated black chert (kink) | 0.04 | –26.09 |
| 275 | 3818-64 | DX F | Massive black chert/red chert alteration | 0.09 | –31.31 |
| 276 | 3818-65 | DX F | Red chert (laminated) | 0.07 | –32.37 |
| 277 | 3818-66 | DX F | Greenish gray silty shale | 0.03 | –23.11 |
| 278 | 3818-67 | DX F | Massive gray chert | 0.01 | –30.14 |
| 279 | 3818-68 | DX F | Greenish gray chert | 0.02 | –26.19 |
| 280 | 3818-69 | DX F | Greenish shale | 0.04 | –17.70 |
| 281 | 3818-69A | DX F | Greenish shale | 0.04 | –16.98 |
| 282 | 3818-69B | DX F | Greenish shale | 0.03 | –17.51 |
| 283 | 3818-69C | DX F | Greenish shale | 0.04 | –19.01 |
| 284 | 3818-69D | DX F | Greenish shale | 0.04 | –17.36 |
| 285 | 3818-70 | DX F | Laminated gray/red chert | b.d. | n.a. |
| 286 | 3818-71 | DX F | Laminated fine sandy chert | b.d. | n.a. |
| 287 | 3818-72 | DX F | Greenish chert (breccia) | 0.02 | –25.06 |
| 288 | 3818-73 | DX F | Greenish shale (massive) | 0.02 | –27.47 |
| 289 | 3818-74 | DX F | Greenish gray chert (breccia) | 0.01 | –24.99 |
| 290 | 3818-75 | DX F | Greenish shale (massive) | 0.02 | –21.77 |
| 291 | 7716-47 | DX F | Black chert vein | 0.01 | –26.81 |
| 292 | 7716-48 | DX F | Black chert vein | 0.01 | –32.22 |
| 293 | 7716-49 | DX F | Black chert vein | 0.01 | –30.09 |
| 294 | 7716-50 | DX F | Black chert vein | 0.02 | –28.57 |
| 295 | 7716-51 | DX F | Black chert vein | 0.01 | –28.54 |
| 296 | 7716-52 | DX F | Black chert vein | 0.01 | –30.77 |
| 297 | 7716-53 | DX F | Black chert vein | 0.02 | –30.01 |
| 298 | 7716-54 | DX F | Black chert vein | 0.02 | –27.48 |
| 299 | 7716-55 | DX F | Black chert vein with quartz vein | 0.03 | –25.42 |
| 300 | 7716-56 | DX F | Black chert vein | 0.02 | –27.85 |
| 301 | 7716-57 | DX F | Black chert vein | 0.03 | –29.34 |
| 302 | 7716-58 | DX F | Black chert vein | 0.02 | –30.52 |
| 303 | 7716-59 | DX F | Black chert vein | 0.03 | –27.37 |
| 304 | 7716-60 | DX F | Black chert vein | 0.02 | –28.96 |

b.d, below detection limits; n.a., not analyzed.

parts of the DX C block are dominated by beds of highly silicified quartz pseudomorphs after aragonite–barite which may account for the low $C_{org}$ contents. The Varicolored Chert Member contains a relatively low proportion of organic-rich rocks.

The $\delta^{13}C_{org}$ contents of black chert veins are constant within each block (–33 to –27‰). The $\delta^{13}C_{org}$ contents of the Black Chert Member are largely between –35 and –30‰, but the middle parts of this member show lower values of between –35 and –45‰ (in the DX A, DX B, and DX D blocks, and in several samples from the DX C and DX E blocks). This trend is particularly clear in the DX B block, where $C_{org}$ changes from 0.3 to 0.5 wt% in the lowermost 5 m to <0.2 wt% at the top of the block. At 5–7 m above the base of the Black Chert Member, there is a negative spike in

the $\delta^{13}C_{org}$ values of –40 to –35‰, which is approximately 10‰ lighter than the average values (–32 to –28‰).

The lateral variations in $C_{org}$ content and $\delta^{13}C_{org}$ values can be summarized as follows. Black chert veins show constant values of $\delta^{13}C_{org}$ (–34 to –25‰). The lower parts of the Black Chert Member have the highest $C_{org}$ contents in this sequence. The $\delta^{13}C_{org}$ values of the lower parts of the Black Chert Member are similar to those of the black chert veins. The middle parts of the Black Chert Member yield relatively low $\delta^{13}C_{org}$ values.

## SEDIMENTARY ENVIRONMENT

The tectonic setting of the Dixon Island Formation has been interpreted as an island-arc setting within an oceanic basin (Kiyokawa *et al.* 2006). Here, we reconstruct the lateral variations in sedimentation during the deposition of the Dixon Island Formation (Fig. 11).

### LATERAL CHANGES IN LITHOLOGY

The sedimentary environment of the Dixon Island Formation was characterized by very low energy and was dominated by the deposition of organic-rich black chert on top of a hydrothermally altered volcanic sequence (Kiyokawa *et al.* 2006). The thickness of the organic-rich black chert beds of the Black Chert Member varies laterally from 5 to 10 m over a horizontal distance of several kilometers. White Tuff 1 varies in thickness from a few meters to 9 m over a similar distance. Even in areas affected by intense hydrothermal alteration, which locally obscures stratigraphic boundaries, the thickness of this tuff bed varies within individual blocks. We suggest that the eastern blocks (DX D, DX E, and DX F) of Dixon Island were located much closer to the center of hydrothermal activity than were the western blocks (DX A and DX B).

Following the cessation of organic-rich hydrothermal activity, silica-rich hydrothermal activity resulted in the deposition of siliceous sediments on the ocean floor, producing very finely laminated chert of the Varicolored Chert Member over a wide area. These cherty rocks formed mainly from the settling of siliceous matter from the ocean.

### EXTENSIONAL DEFORMATION

The tectonic setting during the early to middle stages of deposition of the Dixon Island Formation is reconstructed from the relationship between an early-stage $F_0$ normal fault, black chert veins, and sedimentation of the massive black chert. The fault cuts through a highly altered volcanic zone and the Black Chert Member, indicating it was active after the sedimentation of the Black Chert Member. The fault plane does not contain veins bearing organic matter, and it records only a few meters of offset. This evidence indicates that the fault was not a growth fault that was active during the formation of the Black Chert Member. However, an organic-rich vein in the area has a strike of northwest–southeast (Kiyokawa & Taira 1998), similar to that

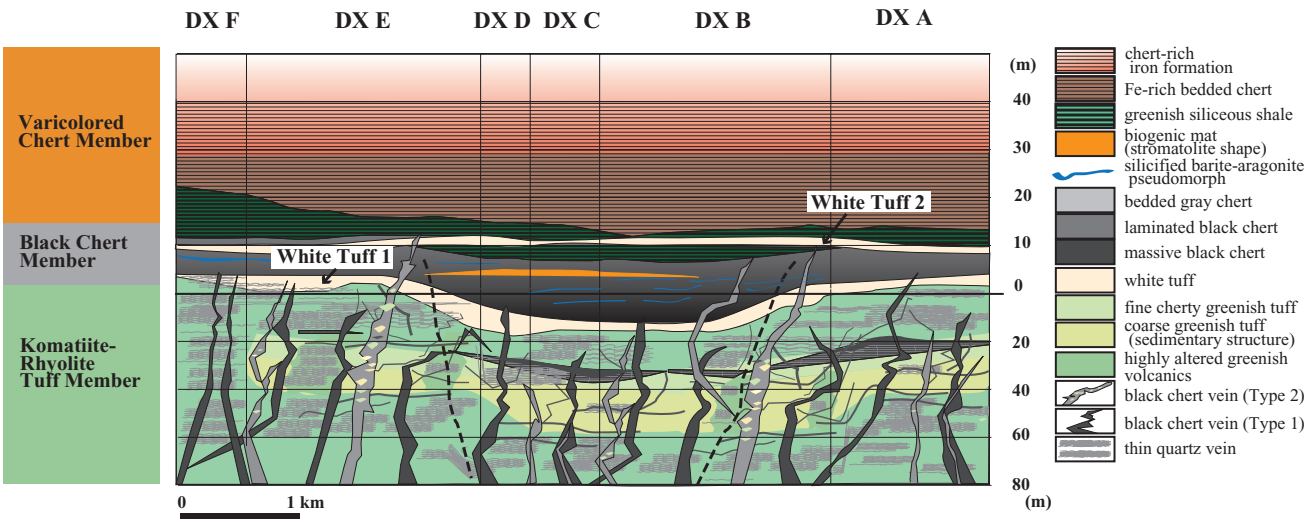


**Fig. 11** Model for sedimentary environment of the Dixon Island Formation.

of the fault. The relative timing of the veining and activity upon the normal fault remains unclear; however, the early-stage black chert vein, the deposition of black chert, and activity upon the $F_0$ normal fault may all have been related to extension within the ocean floor.

## HYDROTHERMAL CIRCULATION

The rocks of Dixon Island contain convincing evidence for hydrothermal circulation below the ocean floor. A highly altered quartz vein swarm and intensive black chert veining within the Komatiite–Rhyolite Tuff Member were produced by hydrothermal circulation in a zone up to several meters wide. Thick, highly altered volcanic sediments and zones characterized by spinifex texture are interpreted as early-stage (relatively hot) hydrothermal pathways. Black chert veins may have been conduits for low-temperature seepage of hydrothermal fluids upon the sea floor. These seepages and hydrothermal vents were subsequently covered by organic-rich cherty sediments.

## CARBON ISOTOPES AND BIOLOGICAL ACTIVITY

The lateral thickness changes in the basal parts of the black chert in the Black Chert Member may indicate a greater output of hydrothermal fluid from the black chert veins. The $C_{org}$ value in black chert of the Black Chert Member is relatively high in the DX B block (>0.5 wt%), and this is the thickest black chert bed in this block. Other blocks yield generally lower $C_{org}$ contents (0.08 wt%), although locally 0.08–0.10 wt%. The exposure of the DX B block is very fresh, in an area subjected to ocean waves. This may explain the high $C_{org}$ contents compared to other blocks; however, the black chert bed in the DX B block is thicker than that in other blocks. The DX B block contains the largest amount of organic mater in the Dixon Island Formation.

Isotopic compositions of $C_{org}$ may be the key to identifying the origin of the organic matter. Most of the $\delta^{13}C_{org}$ values in the black chert bed (massive and laminated) are similar to those in black chert veins ($\delta^{13}C_{org} = -40$ to $-25$‰). Organic matter deposited from the vent system had a higher $C_{org}$ content than did organic matter from the fluid-rich vein system. The high content of organic matter and the thick, massive lithology in the lowermost part of the Black Chert Member indicate that early-stage organic-matter-bearing hydrothermal activity was more intense than during later stages.

Lower values of $\delta^{13}C_{org}$ in the middle parts of the Black Chert Member suggest that additional fractionation (possibly by biological activity) occurred in organic-rich sediments (about 5 m thick) during hydrothermal activity on the paleo-ocean floor. Therefore, the 5-m-thick massive organic-rich beds at the bottom of the member indicate a high rate of precipitation of organic matter in hydrothermal fluids. Beds that retain evidence of intense biological activity inferred from carbon isotope composition at about 5 m from the bottom of the Black Chert Member (these beds are more well laminated than the massive lower black chert) may indicate a lower rate of precipitation of organic matter.

Very finely laminated black chert in the Varicolored Chert Member also indicates a slow rate of sedimentation. The relatively low $\delta^{13}C_{org}$ values of this black chert may be unrelated to organic-rich vein activity. The origin of vertical variations in $\delta^{13}C_{org}$ values in the black chert veins remains unknown.

Biomat beds and microbial fossil structures have been described from the DX B and DX C blocks (Kiyokawa *et al.* 2006). Biogenic, iron-rich mats have been reported around hydrothermal systems at several other sites worldwide (e.g. Iceland; Konhauser & Ferris 1996). Anoxygenic photosynthesizers (purple and green sulfur bacteria) oxidize $Fe^{2+}$ coupled with $CO_2$ reduction (e.g. Ehrenreich & Widdel 1994). The biomat beds of the present study closely resemble modern bacteria in terms of morphology (Kiyokawa *et al.* 2006). We therefore interpret that biological activity occurred within the stagnant organic-matter-rich hydrothermal conditions around the hydrothermal vent systems.

We discovered biomat beds at similar stratigraphic horizons in the DX B, DX C, and DX D blocks. We suggest that these beds formed contemporaneously and that biological activity occurred over an area more than 2 km across. The distribution of biomat beds and their high $C_{org}$ contents are consistent with their occurrence in the thicker black-chert sequences within topographic depressions in the DX B and DX C blocks. The DX A, DX E, and DX F blocks are covered by volcanic rocks (silicified greenish volcanic tuff, siliceous shale, and iron-rich chert layers) and may therefore have experienced less hydrothermal-related biological activity and did not preserve biomat beds.

### BLACK CHERT VEINS AND OCEAN WATER CONDITIONS

Black chert veins have been documented in volcanic rock sequences in Archean greenstone belts elsewhere (e.g. Ueno *et al.* 2004; Lindsay *et al.* 2005; Van Kranendonk 2006). Hydrothermal activity in volcanic rocks produces organic-rich black chert veins under low-temperature conditions. These regional-scale black chert vein systems may introduce hydrothermal fluids into the ocean over a wide area of seafloor. Based on oxygen and silicon isotope analyses, the temperature of the Archean ocean is estimated to have been 55–80°C (Knauth & Lowe 2003; Robert & Chaussidon 2006) or <40°C (Hren *et al.* 2009). In the present study, wide areas of hydrothermal vein activity and the existence of aragonite beds (stable at high temperatures) suggest the ocean temperature near the seafloor was relatively high. Indeed, hydrothermal areas on modern ocean floors, as well as those of Kuroko deposits, commonly contain aragonite- and barite-rich sequences (e.g. Ohmoto 1978; Francheau *et al.* 1979; Shikazono 1983).

### SEDIMENTARY HISTORY

Based on the presence of finely laminated lithologies devoid of detrital materials and the occurrence of non-vesicular glass in felsic volcanics, deposition of the Dixon Island Formation is estimated to have formed at water depths of 500–2000 m (Kiyokawa *et al.* 2006). After komatiite and rhyolite volcanism, hydrothermal activity occurred, producing organic-rich hydrothermal fluids in an area of more than 10 km across. The organic matter in the hydrothermal fluids precipitated on the ocean floor. During a subsequent weakening of organic-rich hydrothermal activity, normal faulting occurred in an extensional setting that is similar to a caldera or rifted volcanic setting, as observed in the modern Izu–Bonin Island-Arc (Smith *et al.* 1990; Taylor *et al.* 1990). However, the relatively minor nature of extensional deformation, small changes in stratigraphic thickness, and absence of detrital fragments indicate that the Dixon Island Formation was deposited in a deep and distal part of a quiescent caldera or in the central part of a rift zone.

## CONCLUSIONS

The Mesoarchean Dixon Island Formation represents a volcanic–sedimentary sequence influenced by syndepositional hydrothermal activity formed in an immature island arc setting. Based on detailed mapping combined with geochemical and carbon isotope analysis of the well-preserved hydrothermal ocean-floor deposits of the formation exposed over a 5 km-wide area on Dixon Island, we reached the following conclusions.

1. Two white tuff layers, which occur within a black chert sequence and are used as marker horizons, allow the identification of lateral variations in the paleo-ocean floor environment within a 5 km-wide section of the Black Chert Member of the Dixon Island Formation.
2. Precipitation from hydrothermal fluids in the Dixon Island Formation was most active within a 1 km-wide area of thick black chert (DX B block).
3. Biomat layers are preserved over a lateral distance of more than 1 km within the DX B, DX C, and DX D blocks, delineating the central portion of the hydrothermal vent system.
4. The lowermost parts of the Black Chert Member contain high contents of organic high carbon with uniform carbon isotope compositions. The lowermost organic-rich chert was precipitated from organic-rich low-temperature fluid (now preserved as black chert veins), producing massive organic-rich sediment on the ocean floor.
5. The black chert veins and Black Chert Member show relatively small variations in carbon isotope composition ($\delta^{13}C_{org}$) (–33 to –27‰), whereas values of –40‰ are found at 5 m above the boundary between the Komatiite–Rhyolite Tuff and the Black Chert Member.
6. Early-stage normal faults cut through highly altered volcanic rocks with thin black chert beds within the Komatiite–Rhyolite Tuff Member. The faults may be related to a caldera or rifting after volcanic and hydrothermal activity in an island-arc setting.

These observations suggest that a >1 km-wide, fault-bound depression on the paleo-ocean floor contained a highly active hydrothermal system and was host to many biomats on the locally anoxic ocean floor. Subsequent to infilling of the depression with organic matter, siliceous and organic matter settled from the seawater column and accumulated as well-bedded chert, blanketing the organic-rich sediments over an area more than 5 km across. The Mesoarchean seafloor was much more diverse in terms of biological activity than traditionally thought.

## ACKNOWLEDGEMENTS

We thank Drs Yasuji Saito, Kazumi Yokoyama, Arthur Hickman, Christian Böhr and Asahiko Taira for discussions. Journal reviewers Jens Gutzmer and Axel Hofmann provided detailed and thoughtful comments. We thank journal editor Professor Yasufumi Iryu for his continued patience and efficient editorial handling. This research was supported by Grants-in-Aid from the Japanese Ministry of Education, Culture, Sports, Science, and Technology (14340153, 18253006, and 22253008). This study was performed under the cooperative research program of Center for Advanced Marine Core Research (CMCR), Kochi University (05A019, 05B002, 06B019).

## REFERENCES

BRAUHART C. W., GROVES D. I. & MORANT P. 1998. Regional alteration systems associated with volcanogenic massive sulfide mineralization at Panorama, Pilbara, Western Australia. *Economic Geology* **93**, 292–302.

BRAUHART C. W., HUSTON D. L., GROVES D. I., MIKUCKI E. J. & GARDOLL S. J. 2001. Geochemical mass-transfer patterns as indicators of the architecture of a complete volcanic-hosted massive sulfide hydrothermal alteration system, Panorama district, Pilbara, Western Australia. *Economic Geology* **96**, 1263–78.

DE RONDE C. E., DE WIT M. J. & SPOONER E. T. 1994. Early Archean (<3.2 Ga) Fe-oxide-rich, hydrothermal discharge vents in the Barberton greenstone belt, South Africa. *Geological Society of America Bulletin* **106**, 86–104.

DE VRIES S. T., NIJMAN W. R. & ARMSTRONG A. 2006. Growth-fault structure and stratigraphic architecture of the Buck Ridge volcano-sedimentary complex, upper Hooggenoeg Formation, Barberton Greenstone Belt, South Africa. *Precambrian Research* **149**, 77–98.

EHRENREICH A. & WIDDEL F. 1994. Anaerobic oxidation of ferrous iron by purple bacteria, a new type of phototrophic metabolism. *Applied and Environmental Microbiology* **60**, 4517–26.

FRANCHEAU J. H., NEEDHAM H. D., CHOUKROUNE P. *et al.* 1979. Massive deep-sea sulphide ore deposit discovered on the East Pacific Rise. *Nature* **277**, 523–8.

HICKMAN A. H. 2012. Review of the Pilbara Craton and Fortescue Basin, Western Australia: Crustal evolution providing environments for early life. *Island Arc* **21**, 1–31.

HORWITZ R. C. 1990. Palaeogeographic and tectonic evolution of the Pilbara Craton, Northwestern Australia. *Precambrian Research* **48**, 327–40.

HREN T., TICE M. M. & CHAMBERLAIN C. P. 2009. Oxygen and hydrogen isotope evidence for a temperate climate 3.42 billion years ago. *Nature* **462**, 205–8.

KITAJIMA K., MARUYAMA S., UTSUNOMIYA S. & LIOU J. G. 2001. Seafloor hydrothermal alteration at Archean mid-ocean ridge. *Journal of Metamorphic Geology* **19**, 583–600.

KIYOKAWA S. & TAIRA A. 1998. The Cleaverville Group in the West Pilbara Coastal Granitoid-Greenstone Terrain of Western Australia: An example of a Mid-Archaean immature oceanic island-arc succession. *Precambrian Research* **88**, 109–42.

KIYOKAWA S., TAIRA A., BYRNE T., BOWRING S. & SANO Y. 2002. Structural evolution of the middle Archean coastal Pilbara terrane, Western Australia. *Tectonics* **21**, 1–24.

KIYOKAWA S., ITO T., IKEHARA M. & KITAJIMA F. 2006. Middle Archean volcano-hydrothermal sequence: Bacterial microfossil-bearing 3.2 Ga Dixon Island Formation, coastal Pilbara terrane, Australia. *Geological Society of America Bulletin* **118**, 3–22.

KNAUTH L. P. & LOWE D. R. 2003. High Archean climatic temperature inferred from oxygen isotope geochemistry of cherts in the 3.5 Ga Swaziland Supergroup, South Africa. *Geological Society of America Bulletin* **115**, 566–80.

KONHAUSER K. O. & FERRIS F. G. 1996. Diversity of iron and silica precipitation by microbial mats in hydrothermal waters, Iceland: Implications for Precambrian iron formation. *Geology* **24**, 323–6.

KRAPEZ B. & BARLEY M. E. 1987. Archean strike-slip faulting and related ensialic basins: Evidence from the Pilbara Block, Australia. *Geological Magazine* **124**, 555–67.

KRAPEZ B. & EISENLOHR B. 1998. Tectonic settings of Archean (3325–2775 Ma) crustal-supracrustal belts in the West Pilbara Block. *Precambrian Research* **88**, 173–205.

LINDSAY J. F., BRASIER M. D., MCLOUGHLIN N. *et al.* 2005. The problem of deep carbon–An Archean paradox. *Precambrian Research* **143**, 1–22.

LOWE D. R. 1999. Shallow-water sedimentation of accretionary lapilli-bearing strata of the Msauli Chert: Evidence of explosive hydromagmatic komatiitic volcanism. *In* Lowe D. R. and Byerly G. R. (eds.) *Geologic Evolution of the Barberton Greenstone Belt, South Africa*, Geological Society of America, Special Paper **329**, pp. 213–32, GSA, Boulder, CO.

LOWE D. R. & BYERLY G. R. 1999. Stratigraphy of the west-central part of the Barberton Greenstone Belt, South Africa. *In* Lowe D. R. and Byerly G. R. (eds.) *Geologic Evolution of the Barberton Greenstone Belt, South Africa*, Geological Society of America, Special Paper **329**, pp. 1–36, GSA, Boulder, CO.

LOWE D. R. & WORRELL G. F. 1999. Sedimentology, mineralogy, and implications of silicified evaporates in the Kromberg Formation, Barberton Greenstone Belt, South Africa. *In* Lowe D. R. and Byerly G. R. (eds.) *Geologic Evolution of the Barberton Greenstone Belt, South Africa*, Geological Society of America, Special Paper **329**, pp. 167–88, GSA, Boulder, CO.

NIJMAN W., DE BRUIJNE K. H. & VALKERING M. E. 1999. Growth fault control of Early Archaean cherts, barite mounds and chert–barite veins, North Pole Dome, Eastern Pilbara, Western Australia. *Precambrian Research* **95**, 247–74.

OHMOTO H. 1978. Submarine caldera: A key to the formation of volcanic massive sulfide deposit. *Mining Geology* **28**, 219–31.

OHTA H., MARUYAMA S., TAKAHASHI E., WATANABE Y. & KATO Y. 1998. Field occurrence, geochemistry and petrogenesis of the Archean mid-oceanic ridge basalts (AMORBs) of the Cleaverville area, Pilbara craton, Western Australia. *Lithos* **37**, 199–221.

ROBERT F. C. & CHAUSSIDON M. 2006. A palaeotemperature curve for the Precambrian oceans based on silicon isotopes in cherts. *Nature* **443**, 969–72.

SHIBUYA T., KITAJIMA K., KOMIYA T. & MARUYAMA S. 2007. Middle Archean ocean ridge hydrothermal metamorphism and alteration recorded in the Cleaverville area, Pilbara craton, Western Australia. *Journal of Metamorphic Geology* **25**, 751–67.

SHIKAZONO N. 1983. Genesis of sulfate minerals in the Kuroko deposit. *In* Horikoshi E. (ed.) *Island Arc, Marginal Seas, and Kuroko Deposit*, Mining Geology, Special Issue **11**, pp. 229–49, The Society of Mining Geologists of Japan, Tokyo (in Japanese with English abstract).

SMITH J., BARLEY M. E., GROVES D. I. *et al.* 1998. The Sholl Shear Zone, West Pilbara: Evidence for a domain boundary structure from integrated tectonic analysis, SHRIMP U-Pb dating and isotopic and geochemical data of granitoids. *Precambrian Research* **88**, 143–71.

SMITH J. R., TAYLOR B., MALAHOFF A. & PETERSEN L. 1990. Submarine volcanism in the Sumisu Rift, Izu-Bonin arc: Submersible and deep-tow camera results. *Earth and Planetary Science Letters* **100**, 148–60.

SMITHIES R. H., CHAMPION D. C., VAN KRANENDONK M. J., HOWARD H. M. & HICKMAN A. H. 2005. Modern-style subduction processes in the Mesoarchaean: Geochemical evidence from the 3.12 Ga Whundo intra-oceanic arc. *Earth and Planetary Science Letters* **231**, 221–37.

TAYLOR B., BROWN G., FRYER P. *et al.* 1990. Alvin-SeaBeam studies of the Sumisu Rift, Izu-Bonin arc. *Earth and Planetary Science Letters* **100**, 127–47.

TERABAYASHI M., MASADA Y. & OZAWA H. 2003. Archean ocean-floor metamorphism in the North Pole area, Pilbara Craton, Western Australia. *Precambrian Research* **127**, 167–80.

UENO Y., YOSHIOKA H., MARUYAMA S. & ISOZAKI Y. 2004. Carbon isotopes and petrography in ~3.5 Ga hydrothermal silica dykes in the North Pole area, Western Australia. *Geochimica et Cosmochimica Acta* **68**, 573–89.

VAN KRANENDONK M. J. 2006. Volcanic degassing, hydrothermal circulation and the flourishing of early life on Earth: A review of the evidence from c. 3490–3240 Ma rocks of the Pilbara Supergroup, Pilbara Craton, Western Australia. *Earth Science Reviews* **74**, 197–204.

VAN KRANENDONK M. J., SMITHIES R. H., HICKMAN A. H. & CHAMPION D. C. 2007. Secular tectonic evolution of Archaean continental crust: Interplay between horizontal and vertical processes in the formation of the Pilbara Craton, Australia. *Terra Nova* **19**, 1–38.